# ACOUSTIC RADIATION FORCE OPTICAL COHERENCE ELASTOGRAPHY : LOCALIZED VS. WIDE-AREA PERTURBATION – A COMPARISON

A Thesis

Presented to the Faculty of the Graduate School

of Cornell University

In Partial Fulfillment of the Requirements for the Degree of

Master of Science

by

Sri nivas Chandrasekaran

February 2016

# ABSTRACT

Elastography is a method to image the biomechanical properties of tissues. The experimental setup has a 10 MHz ultrasound transducer (focal length of 5cm and a spot size of 0.3mm localized excitation and unfocused for wide-area excitation) which generates acoustic radiation force (ARF) to perturb the sample and the corresponding mechanical response is imaged with a spectral domain optical coherence tomography (SD-OCT) with a center wavelength of 800 nm and a bandwidth of 180 nm at a transverse optical resolution of 8μm. The existing hypothesis which states that localized harmonic excitation in audio frequency regime has potential advantages in terms of a better mechanical resolution over wide area harmonic excitation is tested. Contrary to the hypothesis, experimental results demonstrates that wide area harmonic excitation has better mechanical resolution. Further the characterization of the frequency dependence of mechanical contrast establishes that mechanical contrast improves with increasing excitation frequency.

# BIOGRAPHICAL SKETCH

Sri Nivas Chandrasekaran was born on 3rd April 1991 at Chennai, India. He received his Bachelor of Engineering degree in electronics and communication engineering from Anna University in 2012. He is currently working toward the M.S. degree in applied physics at Cornell University.

I dedicate this thesis to my parents Mrs. Lalitha Chandrasekaran and Dr. Chandrasekaran Duraisamy

# ACKNOWLEDGMENTS

First I would I like to acknowledge my masters' thesis advisor Professor Steven Adie for his time, guidance and constant motivation. This thesis would not have been possible without his valuable inputs.

A very special thank you for the current and past members of Adie Lab for their valuable time and help. Gavrielle Untracht for helping me setup the motorized stage scanning and with other issues in LabVIEW, Byung Wook Ryu for setting up the 800nm SD-OCT system, Jeffrey Mulligan for teaching me how to make silicone phantoms and other insightful discussions and Ramin Jafari for helping me with general questions on MATLAB. I would also like to thank all my friends in the student office for their company.

I greatly thank my committee chair Professor Warren Zipfel and other committee member Professor Manfred Lindau for their time, guidance and their valuable feedback.

Finally, I am grateful to my family and friends for all their love, affection, support and motivation.

TABLE OF CONTENTS

LIST OF FIGURES

LIST OF TABLES

# 1. INTRODUCTION AND MOTIVATION

From earlier days, palpation has been used for diagnosis and even today it is used as a part of screening exams in characterizing the condition of different tissues and organs. Major drawback with manual palpation is that it is not quantitative and there is a limitation in the region that can be accessed [1]. After 1980's, many imaging modalities with better imaging abilities evolved, but there remained a wide gap between impressive imaging modalities and minimal information that could be obtained from manual palpation. To fill this gap, a technique named elastography[1] was developed which maps the biomechanical properties of the tissue. Initial elastography experiments were demonstrated using ultrasound modality, where vibrational shear waves were used to perturb the sample and the corresponding mechanical response was imaged using ultrasound.

Elastography is based on three general principles [2]

- Perturbing or exciting the tissue/phantom using a mechanical source.
- Measuring the mechanical response i.e. displacement using suitable imaging modality.
- Quantifying the biomechanical properties from the obtained mechanical response using suitable mechanical models and generating an elastogram.

In this thesis, Acoustic Radiation Force (ARF) (see section 2.5.5) was used to perturb the sample and the corresponding mechanical response was obtained using an in house built spectral domain optical coherence tomography (see section 2.4) system. With varied excitation techniques (see section 2.5), Optical Coherence Elastography (OCE) has different biological and clinical applications. ARF based OCE has been used to detect atherosclerotic plaques and to study age related changes in crystalline lens' biomechanical properties [3]. This technique has its' limitation

for clinical applications due to its limited penetration depth but is well suited for mechanobiology studies at mesoscopic scale like the role of ECM in disease progression [3][4]. ARF based OCE also offers the scope to study effects of harmonic excitation in range of 10 kHz on biological tissues and investigate its viscoelastic properties on that broad range [4].

In elastography, perturbation is usually done over a wide-area of the sample but there have also been studies claiming that perturbation in a localized area has potential advantage over wide-area in terms of mechanical resolution [5]. The primary objective of the thesis is to compare the elastograms from localized palpation over wide-area palpation and experimental validation of the hypothesis which states that remote palpation/localized palpation minimizes the confounding artifacts from reflections from the boundaries and other neighboring heterogeneities and thereby improves the mechanical resolution and provides a more accurate estimate of stiffness in terms of modulus [5],[6].

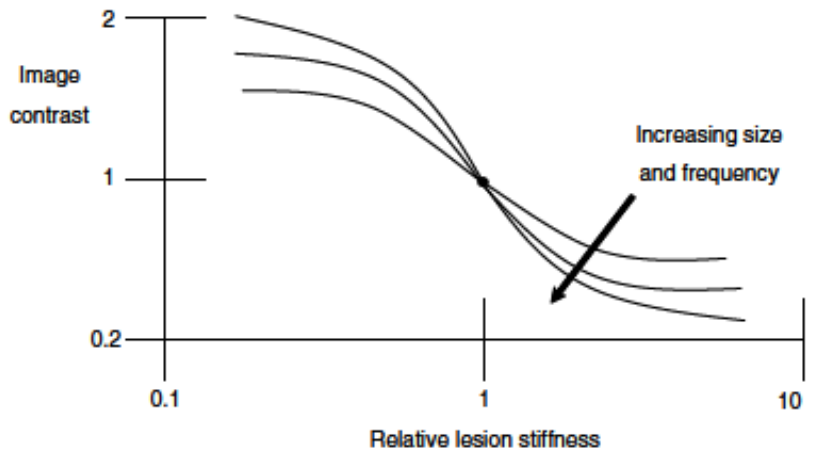


Figure 1.1 : Theoretical Results showing image contrast between lesions of different sizes at different excitation frequencies [7]

The second goal of the thesis is to validate the study [7] shown in Figure 1.1 experimentally which states mechanical contrast between heterogeneities improves with increasing frequency of harmonic excitation and increasing size of the lesion.

# 2. BACKGROUND AND THEORY

In this chapter, the fundamentals and classification of elastography based imaging are discussed. An overview of different techniques to estimate the mechanical properties and mechanical modelling for the purpose of quantifying the estimated mechanical properties are also discussed but the results for quantification and mechanical modelling are beyond the scope of the thesis.

## *2.1 Elastography – an overview*

Elastography is an imaging technique which uses the differences in the biomechanical properties to differentiate the diseased tissue from the normal ones [2]. It provides us with the strain map that can be used to quantify the stiffness of the tissue which in turn is valuable in disease diagnostics [8]. Elastography can be done with different imaging modalities like ultrasound, Magnetic Resonance Imaging (MRI) and Optical Coherence Tomography (see section 2.4) and these modalities determine the resolution of the images that we obtain. Image contrasts in elastography represents the variation in the biomechanical properties of the tissue [9]. Elastography was first developed in the late 1980's to enhance the diagnostic potential of the then existing ultrasound imaging. After its success, it was adopted to MRI and OCT. Elastography is now in its third decade and the first decade saw extensive progress in ultrasound and MRI, only in its second decade it was adopted to OCT. Elastography based on OCT has still not reached the clinical settings but the ultrasound and MRI based elastography technique is used as a diagnostic tool for diseases such as breast cancer, liver cirrhosis, prostate cancer and atherosclerotic plaques [2], [10].

## *2.2 Classification of elastography imaging modalities*

This section briefly discusses different imaging modalities used for elastography based imaging

### *2.2.1 Sono-elastography*

Sono elastography[7] uses low frequency ultrasound shear waves that propagate deep in to the sample, both to perturb the sample and image the mechanical response. Depending on the stiffness of the different parts of the sample, there is a change in the vibration amplitude and phase. The vibration amplitude and difference in phase are estimated by Doppler technique.

### *2.2.2 Magnetic resonance elastography*

MRE[11] is a dynamic technique where mechanical shear waves of audio frequencies are used to perturb the tissue and phase contrast MRI is used to image the mechanical shear waves. In order to estimate the mechanical properties from the response, motion of the shear wave is tracked and inverse techniques are used to estimate the shear modulus with some assumptions such as isotropy, homogeneity and incompressibility.

### *2.2.3 Vibro-acoustography*

In vibro-acoustography[7], two high frequency ultrasound beams of slightly different frequencies are focused at the same spatial location which converts to an acoustic emission of different frequencyand whose frequency is the difference in frequency between two ultrasound beams. The acoustic emission that is radiated perturbs/vibrates the tissue to cause displacement and the corresponding mechanical response is imaged using a hydrophone. ARFI and HMI which also uses radiation force are a variant of this technique.

### *2.2.4 Optical coherence elastography*

OCE uses OCT (interferometric based technique discussed in detail in section 2.4) to image the mechanical response. OCT [10] can image displacements up to a few micro meter resolution. OCT [10] has a higher dynamic range and can image at a depth of 1-2mm. The techniques used to quantify the mechanical properties in OCE are similar to other imaging modalities.

### *2.3 Why optical coherence elastography?*

As shown in Figure 2.1, OCE offers better spatial resolution when compared to sono-elastography or magnetic resonance elastography but penetration depth is low. The first and foremost reason for using OCE to image the mechanical response is that there has been studies claiming that whenever disease occur, there are changes in the extracellular matrix [12]. Extracellular matrix can be imaged with a spatial resolution of 1~10 microns and imaging of ECM will help us to understand the onset of a disease better and thereby helps to prevent it in a very early stage. The other features of OCE [10] are

- OCE has higher 2D acquisition speed in terms of 100's of kHz and thereby has greater potential for 3D in-vivo elastography than other modalities.
- OCE provides sub-nanometer displacement sensitivity and thereby better distinguish even smaller changes in biomechanical properties.
- Even though the penetration depth of OCE is less than that of ultrasound elastography or MRE, this can be overcome by using probes or endoscopy.

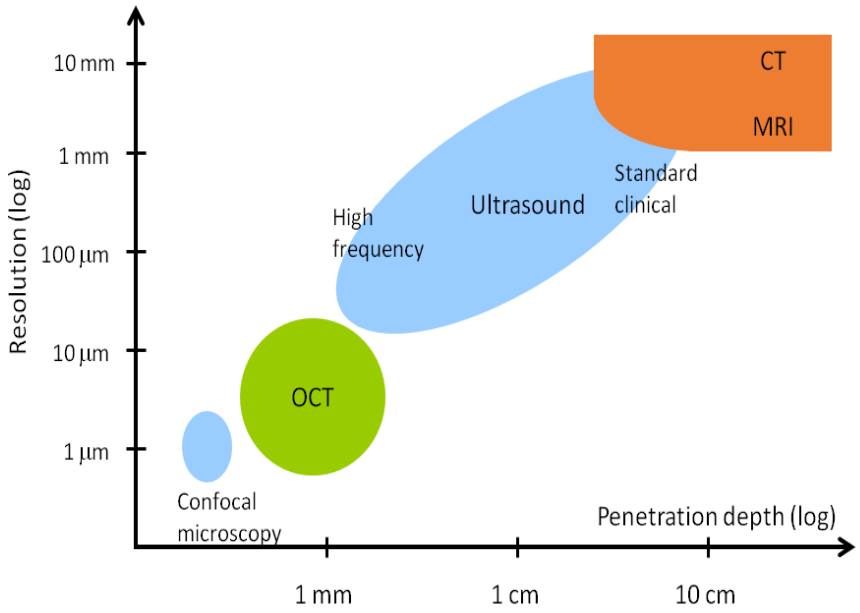


Figure 2.1 : Resolution vs penetration depth comparison for different imaging modlities

### *2.4 Optical coherence tomography – general principle*

Optical coherence tomography [13] can provide 2D image slices at different depths from a three dimensional sample. Optical Coherence Domain Reflectometry (OCDR) from which OCT is based was first used to find defects in fibers but due to its optical sectioning ability, it was then used in ophthalmology and imaging biological tissues. The main features of OCT are 1) it can image at depths that wide field and confocal microscopes cannot image. 2) It can provide us non-invasive in vivo diagnostic images.

An OCT system [14] as shown in Figure 2.2 is based on an interferometric principle. It uses a low coherence source and it has a sample arm and a reference arm. The beam from the source entering the reference arm is subjected to a delay and the reflected light is redirected back in the same path. The beam enters the sample arm via a predefined scanning mechanism which focuses light beam

on the sample in different positions in the lateral direction. The backscattered light from the sample is also redirected in the same path and it interferes with the redirected reference beam and the interference pattern signal is recorded by a line scan camera. The received signal is processed and is finally displayed as either a 2D cross sectional image of the sample or volumetric image of the sample.

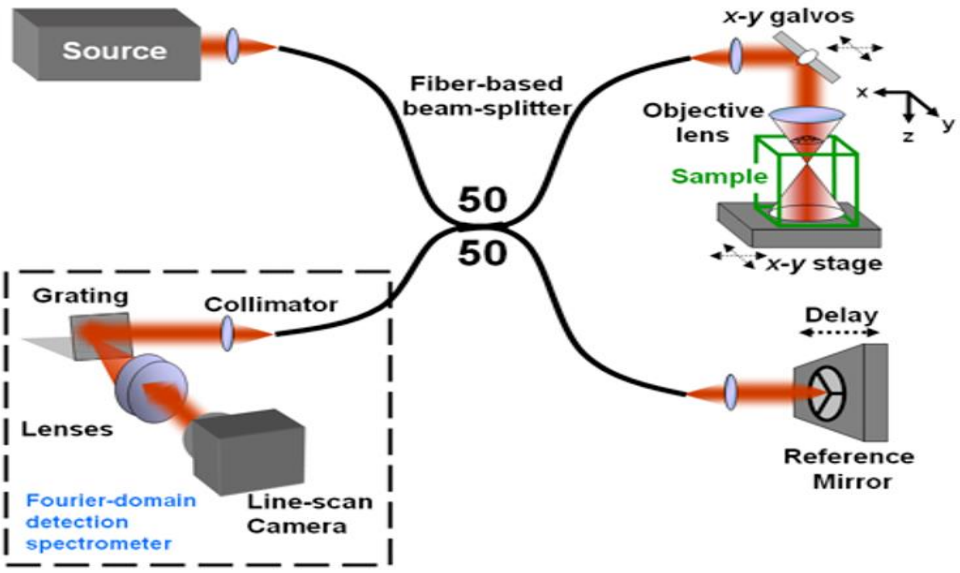


Figure 2.2 : General SD-OCT system setup [15]

### *2.5 OCE techniques*

OCE techniques [10] are classified into static and dynamic based on the type of perturbation. These techniques are also applicable to elastography by other modalities. In static elastography, a strain is induced by a known stress and the corresponding displacement is measured. But static elastography has limitations such as non-uniform distribution of the applied stress. In case of dynamic elastography, a mechanical wave like shear wave is used for perturbation and the propagation of this mechanical wave is tracked. The shear moduli and thereby the stiffness is

quantified from the speed of the tracked mechanical wave [16]. In this section, we will discuss some prominent OCE techniques [10].

| | Static | Dynamic |
|---|---|---|
| External | Compression OCE | Actuator (ring, rod) OCE<br>SAW – OCE |
| Internal | Needle OCE | MM-OCE<br>ARF-OCE |

Figure 2.3 : Summary of different OCE techniques

### *2.5.1 Compression technique*

In compression technique, we perturb the entire region of the sample using an external compressive load. To measure mechanical response we first measure the displacement and thereby calculate the relative strain. But in order to quantify the mechanical response we need to calculate the Young's modulus. Young's modulus is the ratio of stress to strain. We can calculate stress based on indirect prediction based method by matching it with the local strain. In compression technique, entire volume of the sample can be perturbed at once. The spatial resolution of compression OCE is same as the OCT system used.

### *2.5.2 Surface acoustic wave technique*

SAW technique uses surface waves to perturb the sample and these surface waves are detected by the OCT system. There is a relationship between phase velocity of the surface waves and the

Young's modulus which can be used to quantify the mechanical response. The potential features of these SAW techniques are 1) quantification of the mechanical response can be done at an imaging depth exceeding the OCT system 2) perturbation can be done via non-contact method thereby it is suitable for measuring the mechanical properties of delicate tissue like cornea. The limitation is that the lateral resolution is low when compared to compression technique.

### *2.5.3 Magnetomotive technique*

In magnetomotive technique, the magnetic nanoparticles are spread through the sample and energized through an external magnetic field to cause few nanometer displacements. In this technique, the Young's modulus is determined by the time dependence of the motion of magnetic nanoparticels. 2D imaging using this technique was demonstrated in literature [17]. The advantages of MM-OCE is that 1) elastography images can be obtained even from smaller samples since there are no constraints on the geometry of the sample 2) low force perturbation makes it suitable for very soft tissues.

### *2.5.4 Swept frequency loading technique*

In this technique, perturbation is done in terms of a frequency sweep of external loading. This technique is useful in finding the resonant frequency of the sample. Experimental results have demonstrated that the mechanical response from the sweeping frequency loading have detected variation in vibration amplitude and mechanical phase images. The limitation of this method is that it requires to acquire large amounts of data and thereby making it difficult for *in-vivo* implementation.

### *2.5.5 Acoustic radiation force*

Acoustic radiation force is the transfer of momentum to the medium of propagation either by absorption or scattering. The acoustic radiation force F [5] is given by

$$F = (\Pi_a + \Pi_s - \int \gamma \cos\theta \, r dr d\theta) < E > \qquad (2.1)$$

Where $\Pi_a$ is the absorbed power, $\Pi_s$ is the scatterd power, $\gamma$ is the scattering intensity magnitude and $\theta$ is the scattering angle, $<E>$ is temporal average energy density of the propagating wave. ARF can be generated using a standalone ultrasound transducer by modulating the carrier wave in burst mode and the mechanical response due to perturbation can be detected using phase sensitive technique. The advantage of ARF is that precise point loading can be done at specific spatial location of interest.

### *2.6 Potential advantages of focussed excitation*

Acoustic radiation force can perturb the tissue in a localized area and thereby estimate the mechanical properties in that particular region of interest instead of a wide-area. This method is called remote palpation. There has been hypotheses given in the literature [5] which proposes that this remote palpation might have some potential advantages when compared to conventional wide-area perturbation and those potential advantages [5] are listed as follows

- Estimated biomechanical properties are more accurate as the artefacts arising from the boundary due to shear wave reflections have reduced significantly.
- Since ARF is applied directly to the localized area, the force that is needed is less and thereby other regions of the tissue are not exposed to the radiation force.
- At higher excitation frequencies, shear waves have higher attenuation and thereby requires probing the sample response at ultrasound focus. This would provide mechanical decoupling from rest of the sample and thereby would allow us to obtain more accurate estimation of stiffness.

- In localized palpation, imaging of the ARF mechanical response is done in the near field of the shear wave and at higher excitation frequencies it is similar to NSOM providing better contrast but only closer to the surface.
- ARF is used only for a short period of time (few milliseconds), therefore the temperature increase due to heating is less than $1^{o}C$ even with high intensity acoustic beam of $200W/cm^2$. The FDA limit being 0.72 $W/cm^2$ and in our case for localized palpation it is around 2-2.5 $W/cm^2$

### *2.7 Methods to estimate the change in displacement*

Estimating the mechanical response i.e. displacement after perturbation of the sample is of great importance since the accuracy with which the displacement is measured dictates the accuracy of the mechanical properties of the sample. In this section we will discuss about the two prominently used techniques [10] which are speckle tracking and phase sensitive detection.

#### *2.7.1 Speckle tracking*

In OCT, the speckle pattern arises from the back scattering of the sub resolution optical scatters present in the sample. These speckles give the exact location of the scatterers present in the sample. Whenever there is a change in the position of the scatterers, there is a shift in speckle pattern. This shift in the speckle pattern is evaluated using cross correlation method. The advantage of speckle tracking method is that the shift in speckle pattern can be tracked in all 3 dimensions simultaneously. The major drawbacks of this method is that it has lower dynamic range and spatial resolution of estimated displacement is lower than OCT image resolution.

#### *2.7.2 Phase sensitive detection*

Fourier domain OCT and spectral domain OCT provides access to the phase of the signal detected. Unless the sample moves, the phase of the signal detected will remain the same regardless of the

time. In order to estimate displacement, the phase of the sample before and after perturbation needs to be obtained and phase difference should be calculated. There is a direct relationship between displacement and the phase difference which is given in the equation [10] below

$$u_z = \frac{\Delta\varphi\lambda}{4\pi n}\ , \qquad (2.2)$$

where $u_z$ is the displacement, $\Delta\varphi$ is the phase difference, $\lambda$ is the wavelength of the source, n is the average refractive index along the path of the beam. The advantages of phase sensitive detection is that it has a large dynamic range and the spatial resolution is same as the OCT system used. The limitation of this technique is the phase wrapping problem, which can modify the frequency content of the detected signal.

### *2.8 Reconstructing the mechanical properties*

Quantifying the mechanical response [18] gives us the diagnostically relevant information to assess the biomechanical properties of the soft tissue. Soft tissues can be modelled on the basis that it is a viscoelastic medium and it exhibits time dependent mechanical behavior. Viscosity can be used to differentiate healthy tissues rom diseased ones. Several techniques have been developed for the purpose of quantification based on the type of perturbation used. In this section we will cover the quantification technique based on shear wave propagation [18] as we will be using acoustic radiation force to perturb the sample. This section is included to provide an overview of the existing techniques to determine stiffness in terms of modulus but the results are beyond the scope of the thesis.

### *2.8.1 Model-independent reconstruction of shear modulus map*

Considering the soft tissue as viscoelastic medium, we calculate the relaxation shear modulus as the ratio of time dependent stress to the induced strain which is given by

$$G(t) = \frac{\sigma(t)}{\varepsilon}, \qquad (2.3)$$

where $G(t)$ is the relaxation shear modulus and $\sigma(t)$ is the stress and ε is induced strain. When the strain is applied in step, the stress decays with time until it reaches a steady state. Since we use oscillatory excitation via shear waves the shear moduli can be calculated in frequency domain. $G(\omega)$ is complex and is given by

$$G(\omega) = G'(\omega) + iG''(\omega), \qquad (2.4)$$

where $G'(\omega)$ is the storage shear modulus which represents the elasticity of the sample and $G''(\omega)$ is the loss shear modulus and it represents the viscosity of the sample. The wave number k is also complex and it is given by

$$k = k' + ik'' \qquad (2.5)$$

The relationship between wave number $k$ and shear moduli $G$ is given by

$$G = \rho\omega^2/k^2\,, \qquad (2.6)$$

where $\rho$ is the density of the sample and is usually around 1000 kg m $^{-3}$ for soft tissues and ω is the angular frequency. The first step is to equate the real part and the imaginary part of the shear modulus $G$ with the complex wave number *k* using equation *2.6*

$$G' = \frac{\rho\omega^2(k'^2 - k''^2)}{(k'^2 + k''^2)^2} \qquad (2.7a)$$

$$G'' = \frac{-2\rho\omega^2(k'\,k'')}{(k'^2 + k''^2)^2} \qquad (2.7b)$$

From equation *2.7a* & *2.7b*, the imaginary part *k″* i.e. attenuation due to viscosity, which is negative is given by

$$k" = \mathrm{k}'((\mathrm{G}'/\mathrm{G}") - \sqrt{(1 + \frac{G'^2}{G"^2})}\,. \qquad (2.8)$$

The displacement *u(x,t)* as the response to the perturbation by the shear wave propagating along x axis is given by

$$u(x,t) = u_0 e^{i(\omega_0 - kx)}\hat{\mathrm{e}}_z, \qquad (2.9)$$

where $\hat{\mathrm{e}}_z$ represents the direction of the induced displacement.

To obtain the values of *G′* and *G″*, *G′/G″* ratio and *k′* should be determined and it is done experimentally. The real part *k′* which represents the wave propagation is determined by 1D phase gradient computation in the region of interest around the focus. The ratio *G′/G″* is measured by applying an oscillating stress and the corresponding strain is measured. The strain that is measured will also oscillate at same frequency but with a phase delay *φ*. The ratio *G′/G″*, in other words the at focus response is given by

$$G'/G" = 1/\tan(\varphi). \qquad (2.10)$$

The shear modulus that we obtain can be used for diagnosis by correlating it with the clinical information but even more important thing is to try and understand the physical mechanism that causes the change in tissue stiffness [19].

### *2.8.2 Linear viscoelastic mechanical models*

The linear viscoelastic models [20] are represented in terms of spring and dashpot. The spring component represent the elastic behavior of a material. For a spring component *k*, stress is directly dependent on strain.

$$\sigma = k\varepsilon \tag{2.11}$$

The dashpot represents the viscous behavior of the material. For a dashpot component $\eta$, stress is directly dependent on the rate of strain.

$$\sigma = \eta\varepsilon' \tag{2.12}$$

The shear wave phase velocity [21] is associated with viscoelastic properties of the material. The phase velocity is given by

$$c_s = \omega \frac{\Delta z}{\Delta \varphi}, \tag{2.13}$$

where $\omega$ is the angular frequency, $\Delta\varphi$ is the phase shift and $\Delta z$ is the distance over which the phase shift is measured. The shear wave phase velocity [21] can be rewritten as

$$c_s = \omega/k'. \tag{2.14}$$

The two basic viscoelastic models are kelvin-voigt and Maxwell model. In Kelvin-voigt spring component is connected in parallel with the dash pot. In Maxwell model, spring component is connected in series with dashpot.

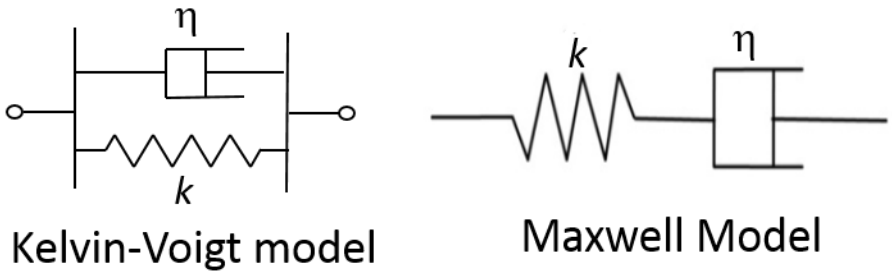


Figure 2.4: Basic linear viscoelastic mechanical models [21]

The phase velocity of kelvin-voigt model [21] is given by

$$c_s(\omega) = \sqrt{\frac{2(k^2+\eta^2)}{\rho(k+\sqrt{(k^2+\omega^2\eta^2)})}}.. \qquad (2.15)$$

The phase velocity of Maxwell model [21] is given by

$$c_s(\omega) = \sqrt{\frac{2k}{\rho(1+\sqrt{(1+k^2/\omega^2\eta^2)})}}. \qquad (2.16)$$

These basic models do not constitute any real material [20]. So different combination of spring and dashpot are used to construct complex standard linear solid models. One such standard linear solid model is Zener model.

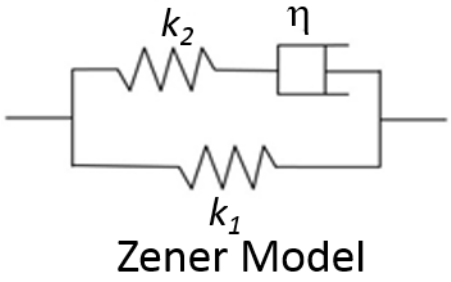


Figure 2.5: Zener model [21]

The shear wave phase velocity of Zener model [21] is given by

$$c_s(\omega) = \frac{\sqrt{2(\omega^2\eta^2(k_1+k_2)^2+k_1^2k_2^2)}}{\sqrt{\rho(\omega^2\eta^2(k_1+k_2)+k_1k_2^2+\sqrt{(\omega^2\eta^2(k_1+k_2)^2)(\omega^2\eta^2+k_2^2)}\,)}}. \qquad (2.17)$$

The shear wave phase velocity at different angular frequencies for a particular material is compared with different constitutive linear viscoelastic model to find a suitable model.

# 3. EXPERIMENTAL METHODS

## *3.1 Experimental setup*

The experimental setup is based on spectral domain OCT system with Ti:Sapphire **(Femtolasers Integral Element)** Laser as the source. The Laser source has a center wavelength of 800nm and bandwidth of 180nm. The OCE system includes ultrasound transducer to generate acoustic radiation force and cause perturbation in the sample. The transducer is of immersion type and is fixed in a water bath at the bottom. The sample is placed in an agar medium to reduce the impedance mismatch between the sample and the water and avoid the sample from absorbing the water and thereby changing its mechanical properties. The ARF push occurs at the top surface of the sample due to impedance mismatch between the top surface and air. It is aligned with the optical beam in the transverse direction.

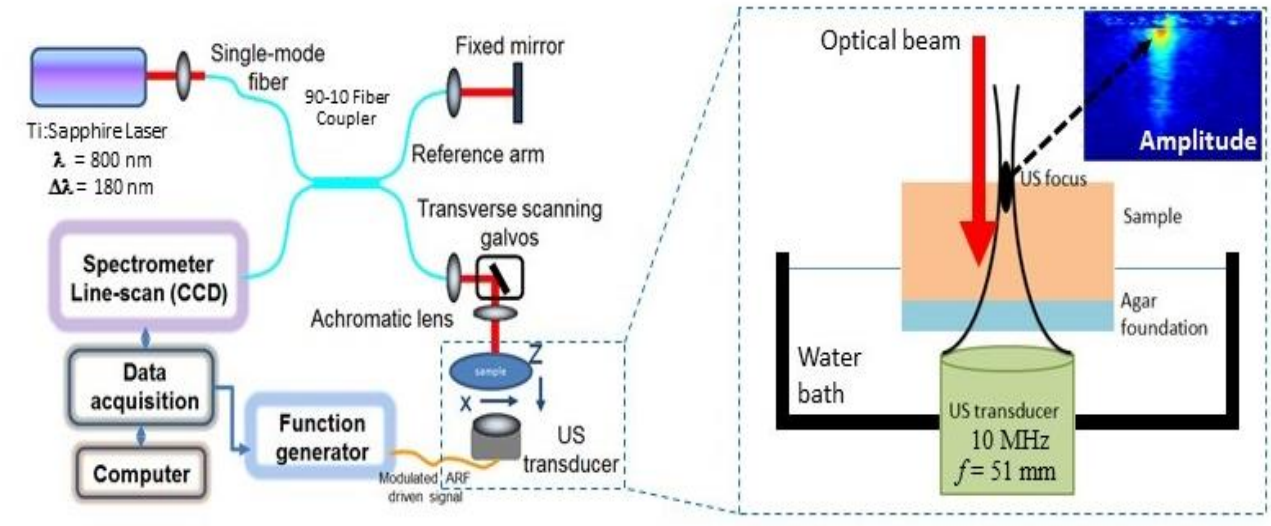


Figure 3.1 : Experimental Setup adapted from [22]

The setup includes a function generator to amplitude modulate the sinusoidal excitation and a 55dB power amplifier **(ENI 3100LA)** to provide required force to cause perturbation. The optical beam is scanned in transverse direction via x-y galvos **(Cambridge Tech)** and controlled by NI DAQ card. The spectrometer **(Wasatch Photonics Cobra)** includes a 4096 pixel line scan camera **(Teledyne Dalsa Piranha 4)** and is connected to PC via NI IMAQ card. The system has numerical aperture of NA =0.1 and has transverse and axial resolution of 8µm and 1µm respectively. The sensitivity of the system is 99dB. Figure 3.1 [22] depicts the entire system setup.

### *3.2 Phantoms with step mechanical contrast*

Gelatin phantoms mimic soft tissues [23]**.** For this experiment, a side-side gelatin phantom of different stiffness/concentrations (i.e. 4%, 6% and 12%) and a side-side silicone – 4% gelatin (shown in Figure 3.2) phantoms are used. The shear moduli of 4% gelatin and 8% gelatin are 571±68 Pa and 2286±315 Pa respectively [24]. The shear modulus of the silicone sample used is 14580±30 Pa [25]. The stiffness of the phantoms used are in the same order as normal adipose and cancerous adipose tissues which are 3500±2200 Pa and 7600±3000 Pa respectively [3].

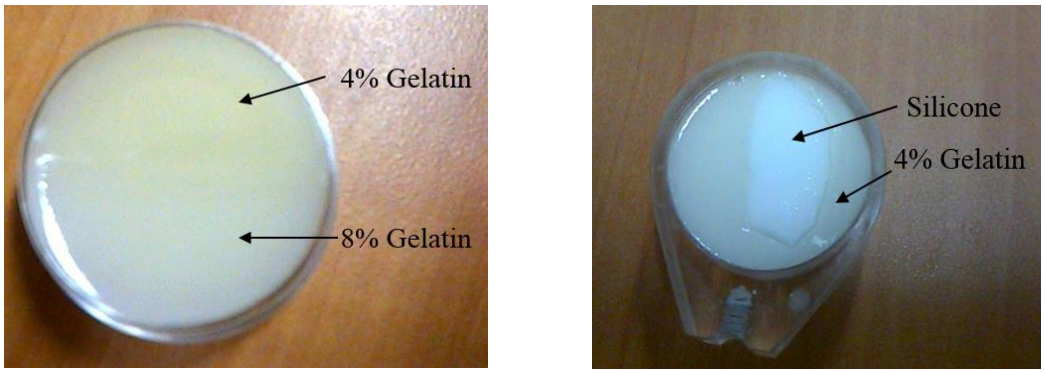


Figure 3.2 : Side by side 4% - 8% gelatin phantom (left) and side-side silicone – 4% gelatin phantom (right)

The procedure [26] for making a side-side 4% and 12% gelatin phantom is as follows. For 12% Gelatin **(Sigma Aldrich Type B G9391)**, use 0.12*100g=12g gelatin power and 88g DI water and mix them together in a beaker. Heat the water bath to 70-80 degree Celsius. Put the beaker into the water bath and cover it to prevent water evaporation. Cook the mixture for 40-45min. In the first 15-20min before the gelatin fully dissolved stir it up and down very slowly with a spoon. Once done, cool the mixture in the room temperature. When the temperature drops to 40 degree, mix them with 0.72 g of $TiO_2$ powder **(US Research Nanomaterials Inc., rutile, high purity, 99.9%, 500nm)**, pour the liquid into a mold. Once 12% gelatin sets, remove one half of the 12% gelatin and pour 4% cooked gelatin mixture (0.04*100g=4g gelatin power and 96g DI water) mixed with 0.72g of $TiO_2$ powder. Allow the 4% gelatin to set. The $TiO_2$ particles are used as optical scatterers.

To make a silicone – gelatin phantom, take the required amount of PDMS (19g) (**ClearCo Products Inc., Polydimethylsiloxane, 50cst**) and add RTV A (**Momentive, RTVA615A01P**) about $1/10^{th}$ of the weight of PDMS and and RTV B (**Momentive, RTVB615A02J**) about $1/100^{th}$ of the weight of PDMS. Add $TiO_2$ (0.09g) depending on the required concentration of the scatterers. Mix the solution for 15 minutes approximately and make sure there are no bubbles on the solution. Pour the mixture in petri dish and cook the solution in the oven at $80^oC$ for 8 hours. Once cooked cut the silicone into small piece and pour the cooked gelatin solution (4% in our case) around it and allow it to solidify.

### *3.3 Perturbing the sample - acoustic radiation force*

Acoustic Radiation Force (see Figure 3.3) is generated by amplitude modulating a negative offset square root of a cosine wave by a 10MHz carrier sine wave (to generate a push to cause

displacement) and sent to the ultrasound transducer. The ultrasound transducer in turn sends the ARF in axial direction to the top surface of the phantom.

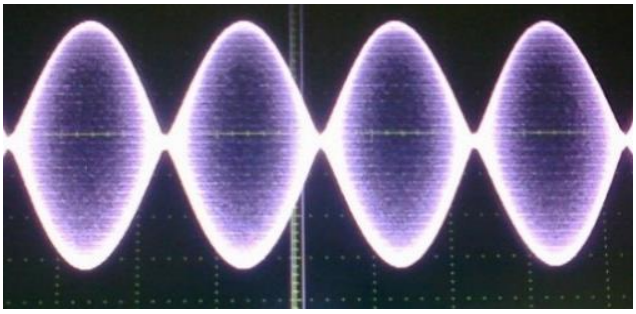

Figure 3.3 : Depiction of Acoustic Radiation Force (Voltage vs Time)

The Acoustic Radiation Force's amplitude and duty cycle are maintained such that the 125mW average power threshold of the ultrasound transducer is met. The modulation wave form signal of the desired excitation frequency is generated from LabVIEW by NI's data acquisition card and the signal is amplitude modulated using a function generator. From the function generator the amplitude modulated signal is sent to the power amplifier and then to the ultrasound transducer. The power amplifier has fixed gain of 55dB so it is important to use attenuators (23dB for the experiments in this thesis) to not send too much power on the amplifier. The modulation signal wave form from the LabVIEW is given by

$$S_m = \sqrt{\frac{A_m}{2}(1 - \cos(2\pi f t)) - \frac{A_m}{2}}. \qquad (3.1)$$

The ARF signal from the function generator after amplitude modulation (obtained from function generator manual) is given by

$$\frac{A_c}{2.2} * \big(1 + m(S_m)\big) * S_c * \big(1 + m(S_m)\big), \qquad (3.2)$$

where $A_c$ and $A_m$ are the amplitude of the carrier and modulation waveform, $S_c$ is the 10 MHz sinewave carrier signal and $m$ is the modulation index.

### *3.4 Imaging the mechanical response (includes stage scanning)*

There are two modes for obtaining the mechanical response, one using unfocused transducer to perturb over a wide transverse field of view and the other using focused transducer to perturb a localized area and perturbation over wide field of view (FOV) for this method is done by scanning the sample and synchronizing it with the imaging system.

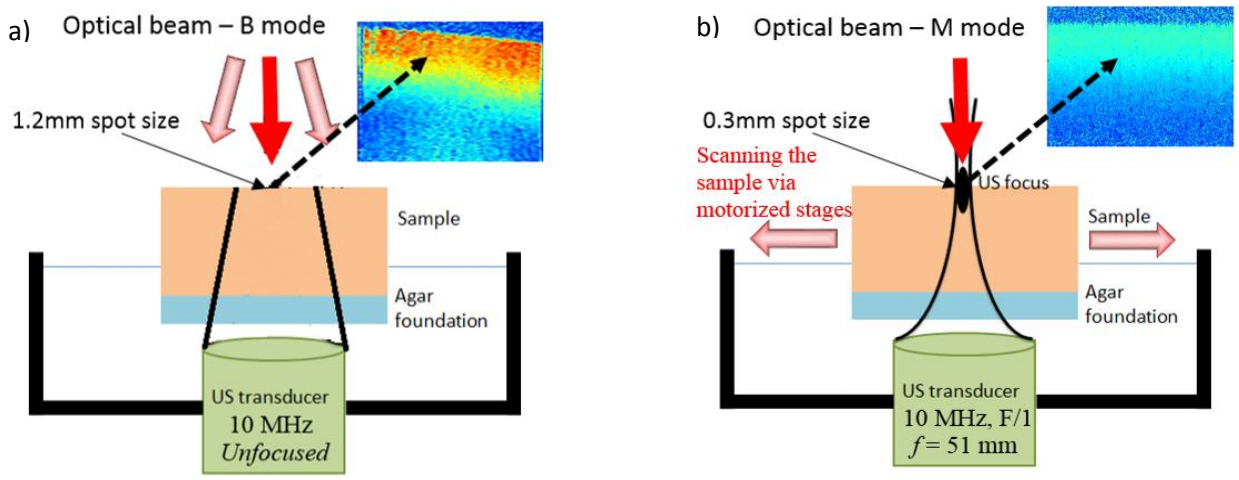


Figure 3.4 : a) Imaging mode for wide perturbation b) Imaging mode for localized perturbation with scanning the sample via motorized stages

#### *3.4.1 Galvo-scanning for unfocused transducer*

The unfocused transducer **(Olympus, 10MHz immersion transducer with 0.25 in. Element Diameter, Unfocused, V312-SU)** is aligned to the optical beam (see Figure 3.4.a). The optical beam is scanned by the galvos for a desired range and a B-Mode OCT image is taken. The mechanical response can be obtained from the phase difference map or vibration amplitude map

of the OCT image. Stiffer the sample, lesser the vibration amplitude. Unfocused transducer provides less force when compared to the focused one.

### *3.4.2 Stage-scanning for focused transducer*

The focused transducer **(Immersion Transducer, 10 MHz, 1.00 in. Element Diameter, F=2.00IN, V322-SU-F2.00IN-PTF)** and the optical beam are aligned (see Figure 3.4.b). Then the sample is scanned using motorized stage **(Newport ILS 50CC)**. The OCT imaging is done using M-Mode and perturbation due to ARF is throughout the imaging FOV. The imaging session starts once the motorized stage reaches a constant velocity and ends when the desired scan range is reached. The scan range corresponds to FOV of the image.

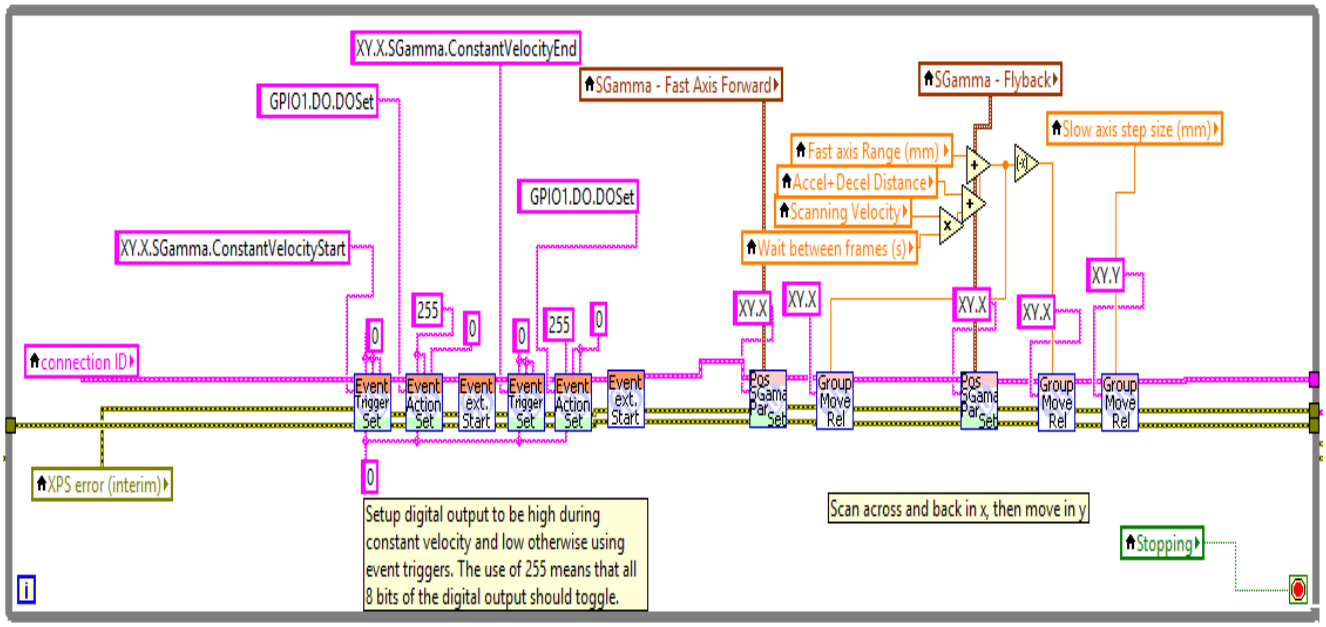


Figure 3.5 : Stage Scanning LabVIEW Block Diagram

The Figure 3.4 depicts the LabVIEW block diagram of the stage scanning procedure. Once this stage scanning module is executed, the motorized x and y stages resets and goes back to its initial position. First an event trigger and event action is set for the imaging to begin when the stage

reaches a constant velocity. Here the event trigger is “constant velocity start” and event action is that GPIO bits are changed to 11111111 from 00000000. Event extended start activates the event. Similarly when to end the imaging session, event trigger is set to “constant velocity end” and the event action sets GPIO bits back to 00000000. The event is activated using event extended start. The scanning distance, velocity and acceleration are input using SGammaParameterSet command. There is fly back scanning which corresponds to the wait time between the frames which is needed to maintain the average power of the transducer and reduces the duty cycle of the ARF push signal. Once the flyback is over, the stage returns to its original position and repeats the same steps for the next frame.

### *3.5 Mechanical resolution and contrast*

Mechanical resolution refers to the degree of sharpness at which the boundary of a heterogeneity can be found in the elastogram whereas mechanical contrast refers to the ratio of displacements between regions of different stiffness due to perturbation. t\The boundary between heterogeneities which often in experimental measurements is a gradient of varying vibration amplitude/ displacement and is not used in the calculation of mechanical contrast. The mechanical resolution for optical coherence elastography depends on experimental acquisition parameters and is limited by imaging system resolution and the following equation.

$$\frac{Number\ of\ cycles}{\mu m} = \left(\frac{Excitation\ Frequency}{Linescan\ rate}\right) * \left(\frac{Numberof Ascans}{FOV}\right) \quad (3.3)$$

Mechanical resolution is quantified by calculating the Full Width Half Maximum (FWHM) of the gradient of normalized vibration amplitude over the desired FOV (i.e. impulse response). It is important to maintain the number of cycles/ μm from equation 3.3 as constant during the

experiment to study the effects on mechanical resolution and contrast while varying factors like excitation frequency and number of Ascans (see section 4.3).

### *3.6 Data processing*

The procedure for data processing was adapted from the literature[27]. The raw OCT signal is in spectral domain and undergoes background subtraction, dispersion correction, k-space resampling and Fourier transformation. The complex OCT signal with ARF perturbation at the angular frequency $\Omega$ is given by

$$\tilde{S}(x,z,\Omega) = \widetilde{S_0}(x,z,\Omega)e^{i\varphi(x,z,\Omega)}, \quad (3.4)$$

where $x$ is the transverse position, $z$ is the depth, $\varphi(x,z,\Omega)$ is the optical phase and $S_0(x,z)$ is the complex OCT signal with no ARF perturbation. The optical phase derivative is obtained by calculating the phase difference between adjacent A scans and is given by

$$\tilde{S}(x+dx,z,\Omega)\widetilde{S^*}(x+dx,z,\Omega) = e^{i[\varphi(x+dx,z,\Omega)-\varphi(x,z,\Omega)]}, \quad (3.5)$$

$$\Delta\varphi(x,z,\Omega) = \varphi(x+dx,z,\Omega) - \varphi(x,z,\Omega), \quad (3.6)$$

where $dx$ is the separation between adjacent A-scans.

The next step is signal conditioning which includes median filtering, low pass filtering to minimize the phase noise. Phase wrapping is another factor which results in phase noise. Phase wrapping occurs when the phase velocity crosses the (-π, π) limit and the waveform wraps itself in the process of doing so. This results in a shift in the frequency content of the vibration signal. In order

to correct for phase wrapping, we would need special phase unwrapping techniques. To maintain the phase shift within the limit, the following condition should be satisfied.

$$-\pi < \frac{m\, v_z(x,z,\Omega)}{f_{Ascan}\left(\frac{\bar{\lambda}}{4\pi n}\right)} < \pi, \qquad (3.7)$$

where $m$ is the number of Ascans with which phase difference is calculated. $v_z\,(x, z, \Omega)$ is the sample's axial velocity and $f_{Ascan}$ is the frequency at which each scan was taken.

Bandpass filtering is applied to reduce the residual phase noise. Once the conditioning and filtering is done, a displacement map is generated by integration of phase difference over the spatial region and multiplying with $\bar{\lambda}/4\pi n$ term. The relationship between optical phase and local displacement is given by

$$d(x,z,\Omega) = \left(\frac{\bar{\lambda}}{4\pi n}\right)\int_0^x \Delta\varphi(x',z,\Omega)dx', \qquad (3.8)$$

where $\bar{\lambda}$ is the optical wavelength and $n$ is the refractive index of the material. The complex displacement is projected in terms of vibration amplitude map. Figure 3.5 [27] summaries the data processing steps.

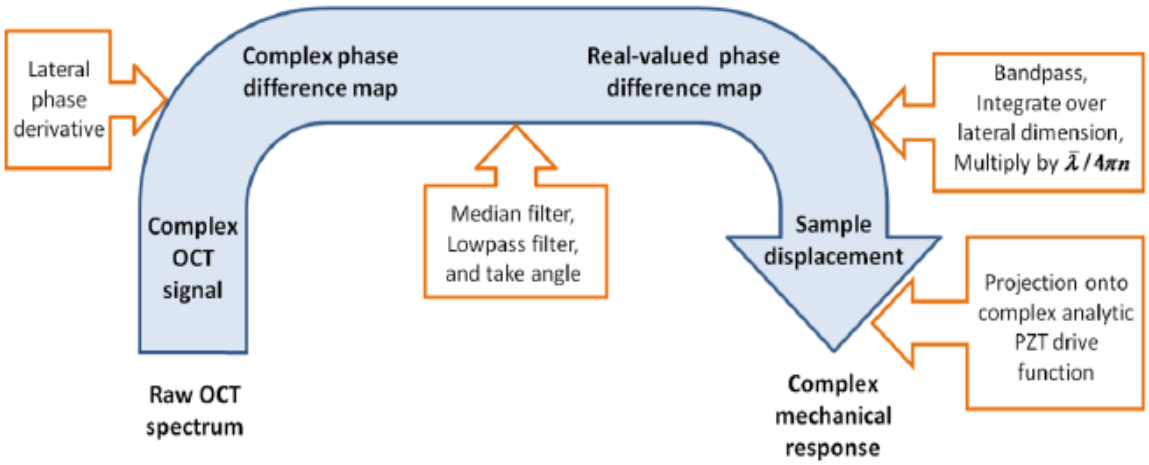


Figure 3.6 : Steps for processing the OCT data [27]

# 4. RESULTS AND DISCUSSION

In this chapter, we will discuss the frequency dependence of mechanical contrast for localized and wide-area excitation results first and then compare the mechanical contrast and resolution between localized and wide-area excitation.

### *4.1 Mechanical interaction length*

Mechanical Interaction Length (MIL) is defined as the full width of the propagating shear wave amplitude at the 1/*e* level. The figure 4.1 (Experimental data obtained from Biophotonics Imaging Laboratory, UIUC) shows the normalized shear wave amplitude vs. transverse position at a depth of 160µm for different excitation frequencies in a 4% homogenous gelatin sample. The results show that the MIL reduces with increasing excitation frequency and reduced MIL is expected to provide better mechanical contrast since increasing excitation frequency has higher attenuation and thereby provides better mechanical decoupling from other heterogeneities in the sample and reduce reflection artifacts from the boundaries.

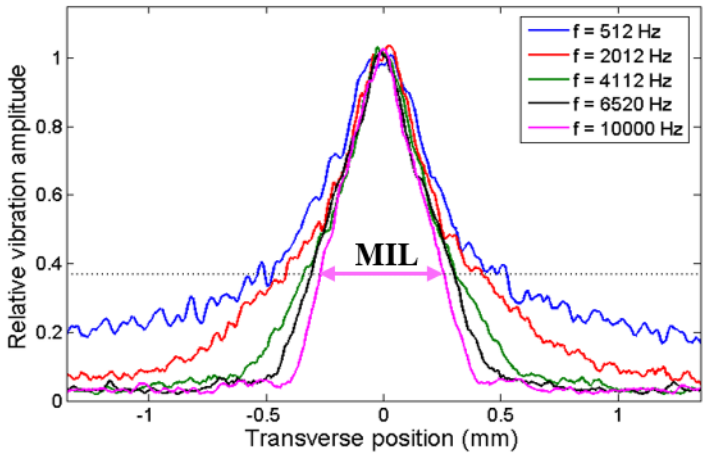


Figure 4.1 : Frequency dependent mechanical interaction length

### *4.2 Frequency dependence of mechanical contrast*

The validation of frequency dependence of mechanical contrast is shown with both wide-area and localized excitation techniques.

#### *4.2.1 Localized excitation*

The localized excitation experiment is performed by aligning the ultrasound beam focus to the top surface of the sample and aligning the optical beam and ultrasound beam to the same position laterally. Once the alignment is done, the sample is scanned using motorized translation stages such that the whole scan region is perturbed locally (refer to section 3.4.2 and Appendix A for more details). The experimental parameters used for this experiment are provided in the Table 4.1. Figure 4.2 represents the mechanical response (i.e. displacement) of localized excitation at 2000Hz excitation frequency on 8% homogenous gelatin sample using imaging configuration mentioned in section 3.4.2. Figure 4.3, 4.4 and 4.5 represents the mechanical response on a side - side 12% - 6% gelatin phantom at excitation frequencies of 500 Hz, 2000 Hz and 6000 Hz respectively. Figure 4.6 shows the normalized vibration amplitude plot of single row over the field of view and it demonstrates that the mechanical contrast between two regions of different stiffness improves with increasing excitation frequency. As shown in Figure 4.1 the attenuation of propagating shear wave increases with increasing excitation frequency and thereby the depth at which a sample's biomechanical properties can be reconstructed reduces with increasing excitation frequency (provided sample is perturbed at the top surface). It is also seen from Figure 4.5 and Figure 4.6, at excitation frequencies of 4000 Hz and higher, there is no perturbation at the boundary between two regions of different stiffness and thereby providing a better mechanical contrast. Figure 4.6 also demonstrates that mechanical contrast between heterogeneities improves with increasing excitation frequency.

Table 4.1: Experimental parameters and phantoms used for localized excitation experiments (frequency dependence)

| Excitation and imaging | Localized with stage scanning and M-mode imaging |
|---|---|
| Sample1 | 8% Gelatin (Homogenous) |
| Sample2 | Side-side 12% - 6% Gelatin sample |
| Number of Ascans | 4096 |
| Field of view (Transverse) | 1.078mm |
| Field of view (Axial) | 2mm |
| Excitation Frequency | 500Hz – 6000Hz |

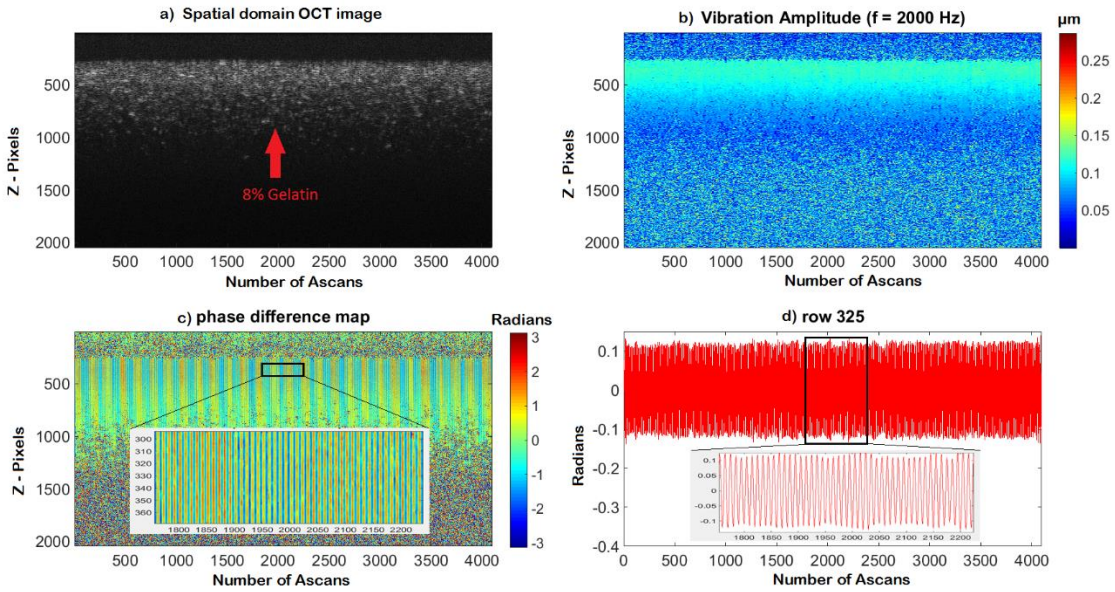


Figure 4.2 : Localized excitation with stage scanning at 2000Hz excitation frequency on a homogeneous 8% gelatin sample (Sample1).

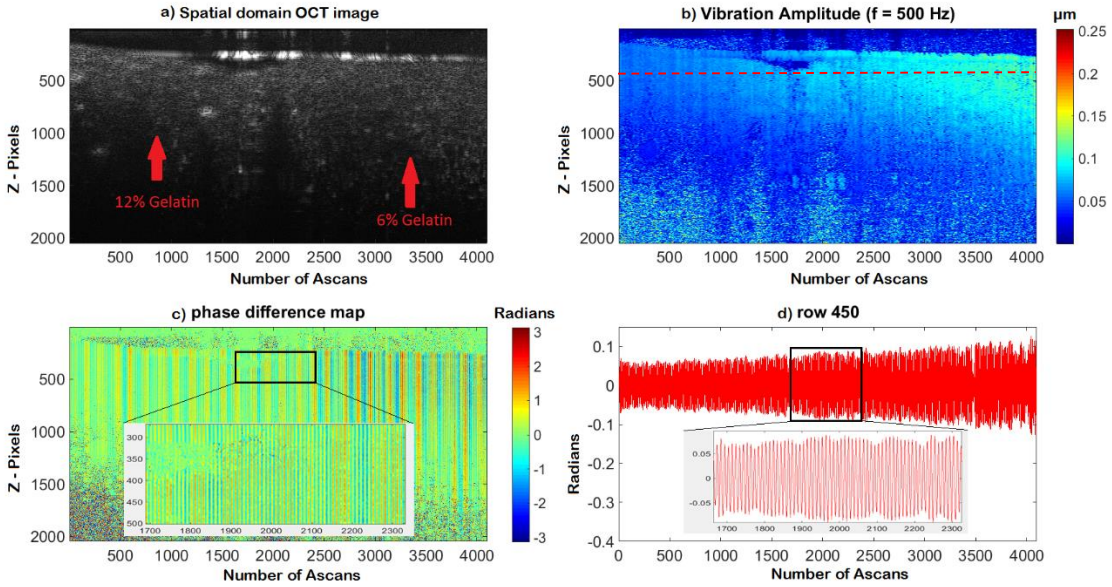


Figure 4.3 : Localized excitation with stage scanning at 500Hz excitation frequency on a side-side 12% -6% gelatin sample (Sample 2) (The dashed red line points to the row plotted in Figure 4.6)

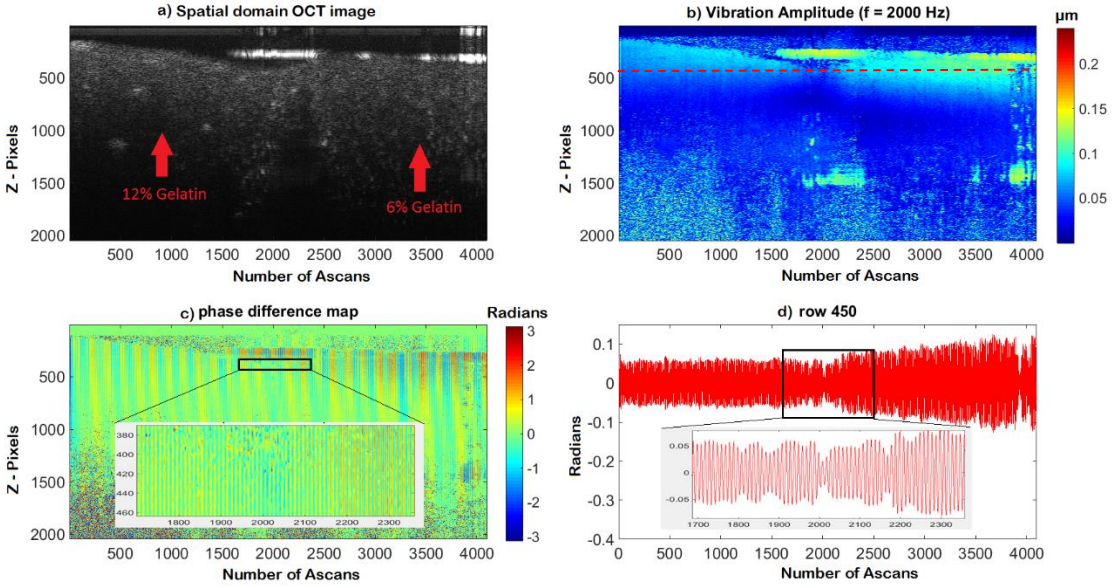


Figure 4.4 : Localized excitation with stage scanning at 2000Hz excitation frequency on a side-side 12% -6% gelatin sample (Sample 2) (The dashed red line points to the row plotted in Figure 4.6)

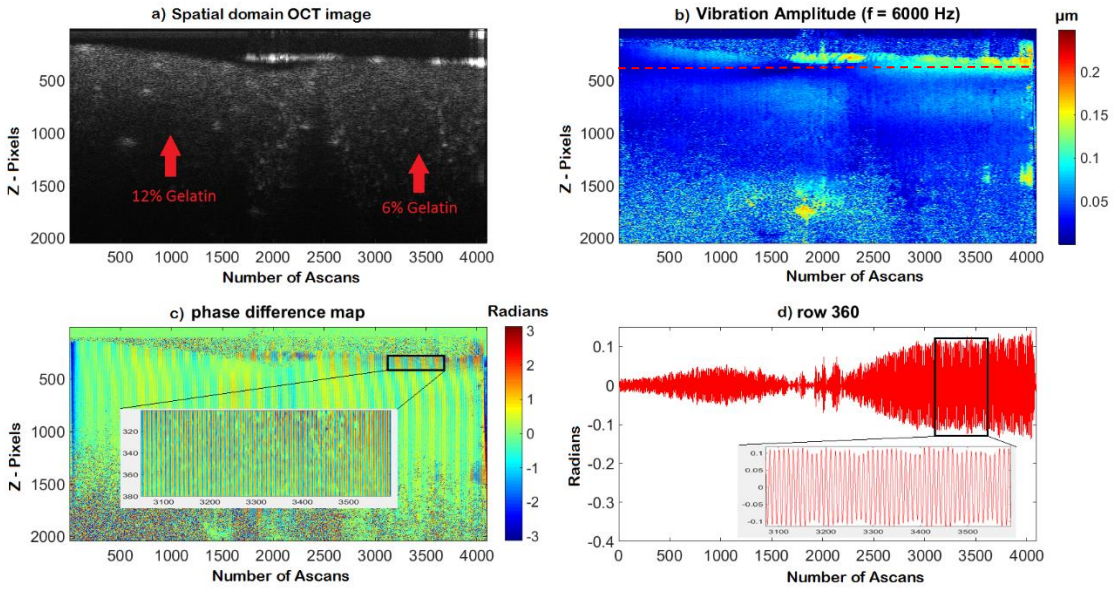


Figure 4.5 : Localized excitation with stage scanning at 6000Hz excitation frequency on a side-side 12% -6% gelatin sample (Sample 2) (The dashed red line in points to the row plotted in Figure 4.6)

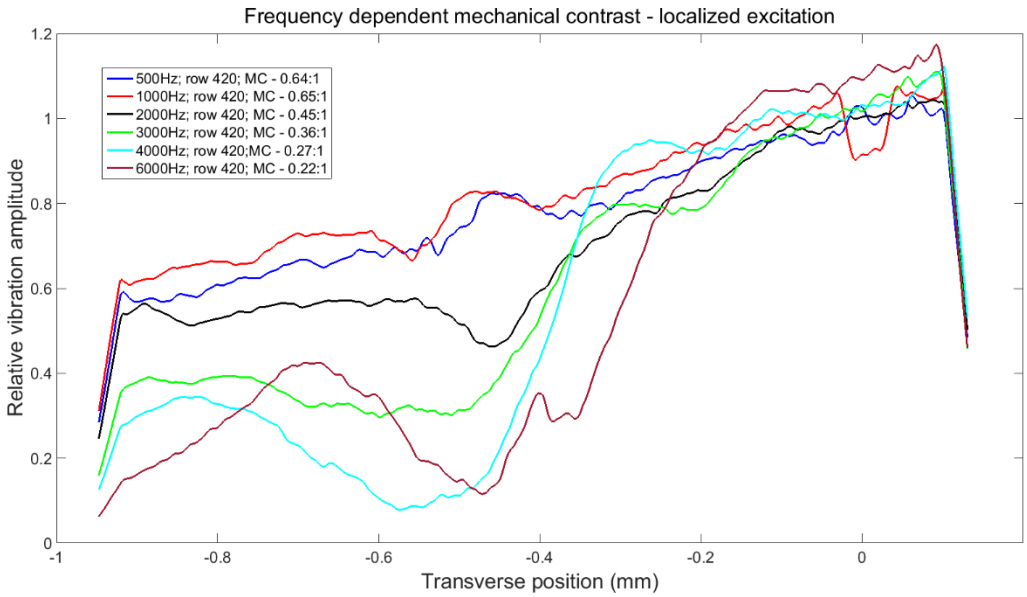


Figure 4.6 : Frequency dependent localized excitation with stage scanning at excitation frequencies 500Hz to 6000Hz on a side-side 12% -6% gelatin sample (Sample 2); MC refers to Mechanical Contrast

### *4.2.2 Wide-area excitation*

The wide-area excitation is performed using an unfocused transducer and exciting the bulk of the sample. The region of the excitation depends on the spot size of the beam and the interaction length which in turn depends on the excitation frequency. The imaging technique used is B-mode i.e. scanning the optical beam (refer to section 3.4.1 and Appendix A for more details). The experimental parameters used for this experiment are provided in the Table 4.2. Figure 4.7 represents the mechanical response of wide-area excitation at 500Hz excitation frequency on 4% homogenous gelatin sample using imaging configuration mentioned in section 3.4.1. Figure 4.8, 4.9 and 4.10 represents the mechanical response on a side-side 4%-12% gelatin phantom at excitation frequencies of 300 Hz, 800 Hz and 1200 Hz respectively. Similar to the results seen in section 4.2.1 for localized excitation, figure 4.11 shows that with increasing excitation frequency the mechanical contrast between regions of varying stiffness increases for a wide-area excitation. Since attenuation is higher with increasing excitation frequency, at 1200Hz and above, doesn't perturb the whole FOV (1.078 mm) which is shown in figure 4.10 and 4.11. Figure 4.11 also demonstrates that mechanical contrast between heterogeneities improve with increasing excitation frequencies.

Table 4.2: Experimental Parameters and phantoms used for wide-area excitation experiments (frequency dependence)

| Excitation and imaging | Wide-area with B-mode Imaging |
|---|---|
| Sample1 | Gelatin 4% Sample (Homogeneous) |
| Sample2 | Side-side 4% - 12% Gelatin sample |
| Number of Ascans | 2048 |
| Field of view (Transverse) | 1.078mm |
| Field of view (Axial) | 2mm |
| Excitation Frequency | 200Hz – 1200Hz |

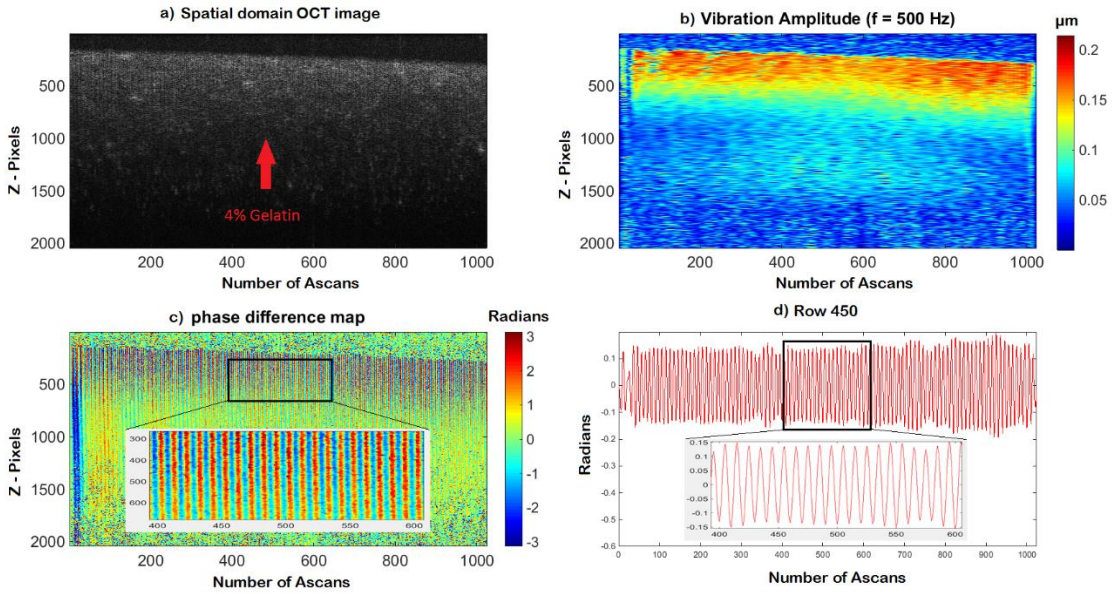


Figure 4.7 : Wide-area excitation at 500Hz excitation frequency on a homogeneous 4% gelatin sample (Sample 1)

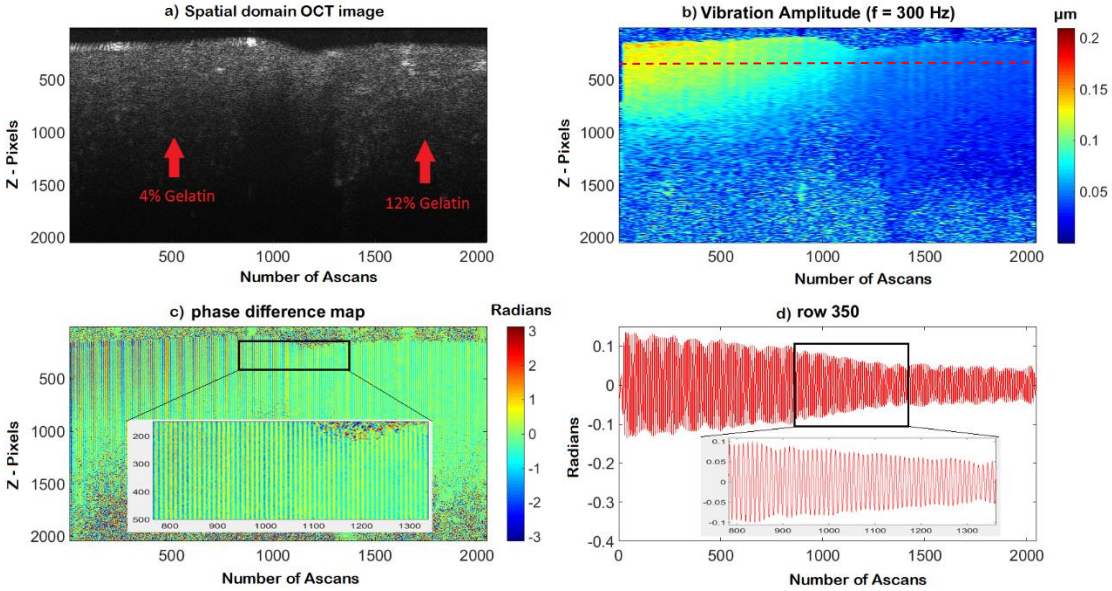


Figure 4.8 : Wide-area excitation at 300Hz excitation frequency on a side-side 4% -12% gelatin sample (Sample 2)
(The dashed red line refers to the row plotted in Figure 4.11)

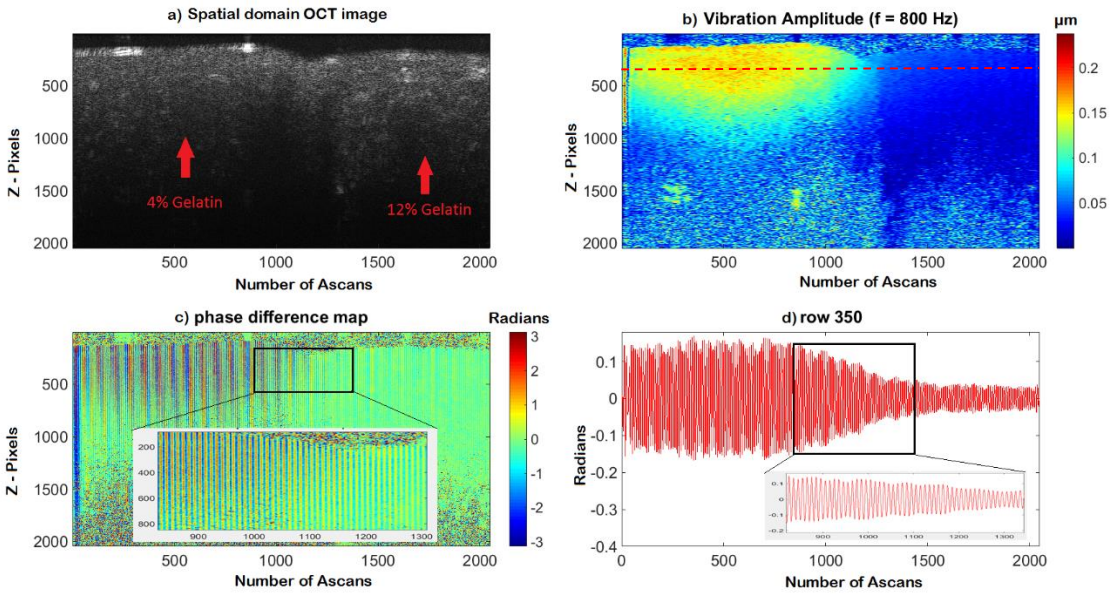


Figure 4.9 : Wide-area excitation at 800Hz excitation frequency on a side-side 4% -12% gelatin sample (Sample 2) (The dashed red line refers to the row plotted in Figure 4.11)

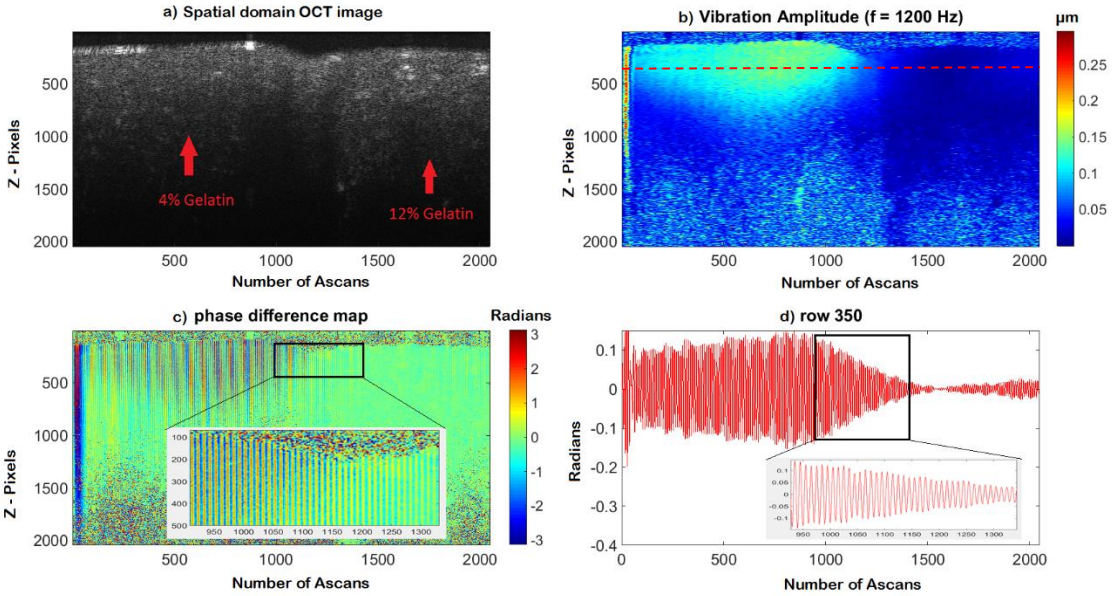


Figure 4.10 : Wide-area excitation at 1200Hz excitation frequency on a side-side 4% -12% gelatin sample (Sample 2) (The dashed red line refers to the row plotted in Figure 4.11).

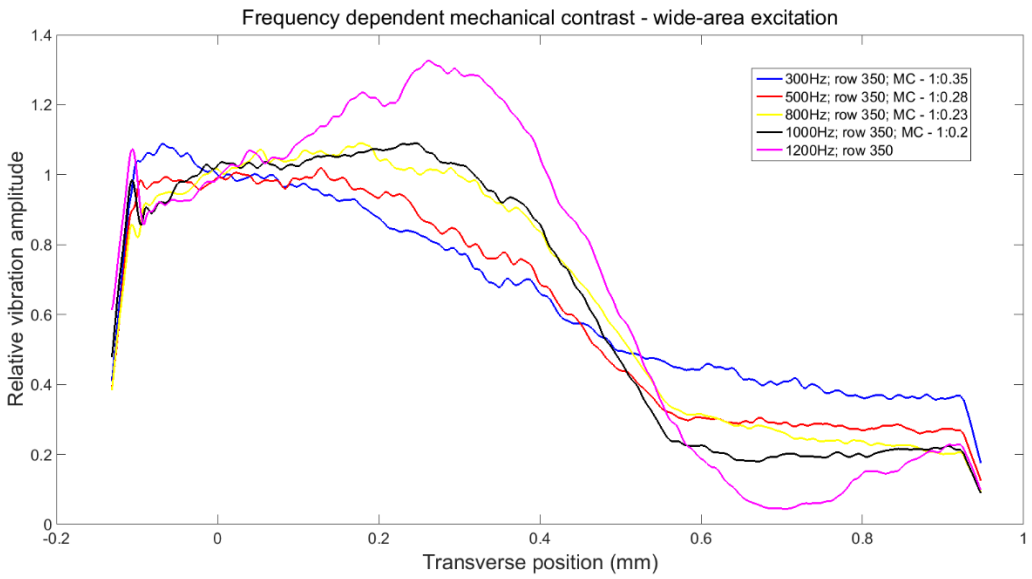


Figure 4.11 : Frequency dependent wide-area excitation at excitation frequencies 300Hz to 1200Hz on a side-side 4% -12% gelatin sample (Sample 2); MC – Mechanical Contrast; (Higher attenuation with increasing excitation frequency resulted in not perturbing the whole FOV at 1200 Hz and above )

### *4.3 Other factors affecting the mechanical contrast*

There are factors other than the excitation frequency such as number of Ascans, bandwidth of the filter and Ascan rate that affect the mechanical contrast.

#### *4.3.1 Change in mechanical resolution and contrast with change in number of a-scans and a-scan rate*

As discussed in section 3.5, the mechanical resolution and contrast increases with higher the number of A-scans as sampling points within the FOV increases. When the A-scan rate is decreased, the mechanical resolution increases (see Equation 3.3) provided the ratio between A-scan rate and excitation is higher than the Nyquist limit. Experimentally, the ratio should be a minimum of 5 due to over sampling. From the results shown in this chapter, the ratio is kept constant throughout at 10.

### *4.3.2 Change in mechanical contrast with the bandwidth of the filter*

The motorized stages when scanning the sample introduces other stray frequency components which interfere with the excitation frequency and affect the SNR of the phase map and thereby the vibration amplitude map. This case is specific to localized excitation as the in case of wide-area excitation the optical beam is scanned instead of scanning the sample. The frequency of the components that arise from scanning the motorized stage, varies with the velocity at which it scans. This effect is prominent in low excitation frequencies (200-800 Hz) but not in higher excitation frequencies (above 1 kHz) as stray frequencies coincide with the low excitation frequencies. One way to overcome this is to use a narrow band bandwidth filter (butterworth filter in this case). The trade off in deciding the bandwidth of the filter is to not lose any information from the applied harmonic excitation but to filter out the stray components. Figure 4.12 and 4.13 show how the stray frequency components affect the SNR of the phase map and the displacement map at different bandwidth of the filter used. The selection of bandwidth is determined with respect to ratio of the A-scan rate to the excitation frequency. Since that ratio is kept constant, the bandwidth of the filter is also kept constant for different excitation frequencies.

Table 4.3: Experimental parameters and phantom for the effect of bandwidth of the filter on mechanical contrast

| Sample | Side-side Silicone and 4% Gelatin sample |
|---|---|
| Number of Ascans | 2048 |
| Field of view (Transverse) | 1.078mm |
| Field of view (Axial) | 2mm |
| Excitation Frequency | 600Hz |

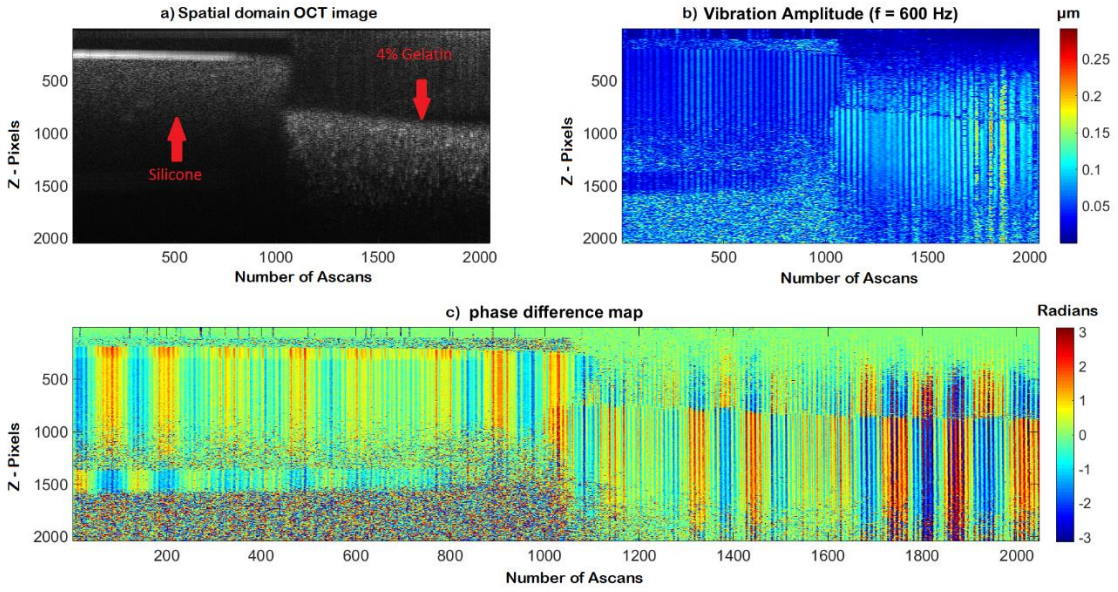


Figure 4.12 : Localized excitation with stage scanning at 600Hz excitation frequency on a side-side silicone -4% gelatin sample with a wide band butterworth filter

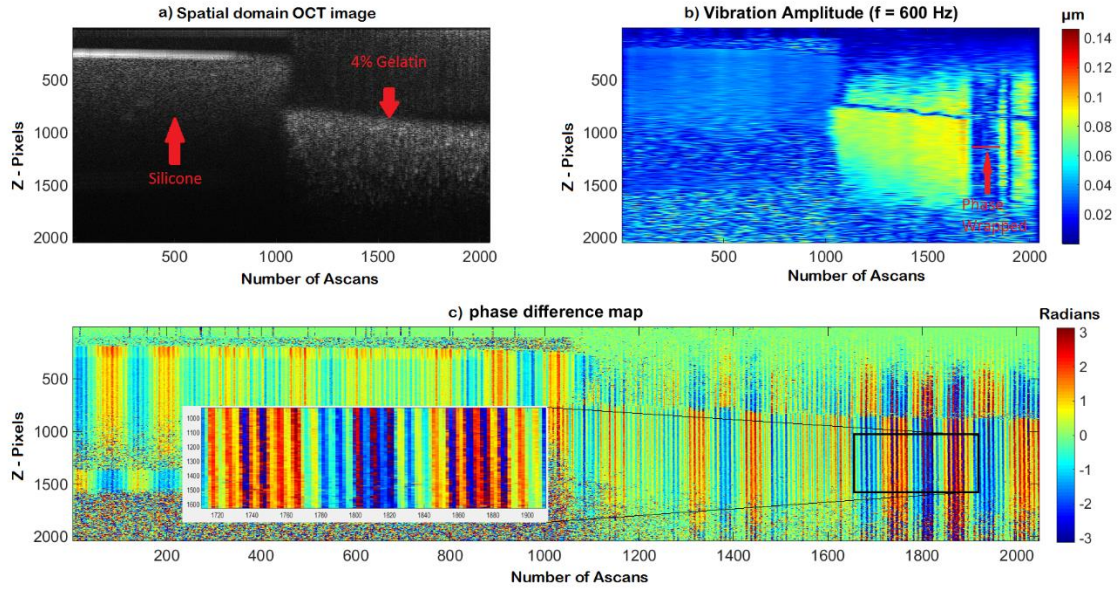


Figure 4.13 : Localized excitation with stage scanning at 600Hz excitation frequency on a side-side silicone -4% gelatin sample with a narrow band butterworth filter.

### *4.4 Comparison of localized excitation versus wide-area excitation*

For comparing localized versus wide-area excitation, all the experimental parameters were kept the same (see Equation 3.3 and Section 3.5). This experiment was performed in a side-side silicone - 4% gelatin sample. The experimental parameters used for these experiments are provided in Table 4.4. Both these methods cause perturbation at the near field of the excitation (for frequency ranges that's been used). The main difference between wide-area and localized excitation is that in case of wide-area, the perturbation is bulk and it would add to additional transverse displacements which in turn would contribute to the axial displacements that's measured. The reason for using a silicone and gelatin sample rather than a side-side gelatin of two different stiffness is that silicone is hydrophobic and provides a sharp mechanical boundary with the gelatin. The same sample was used for both methods and the experiments were performed on the same day (approx. 4hrs for both methods). Different regions of the same sample were probed to establish consistency in the results. Figure 4.24 and 4.25 show that there are no frequency dependent mechanical contrast for silicone –gelatin sample which contradicts the frequency dependence seen in side-side gelatin sample. Figure 4.14, 4.15, 4.16, 4.17, 4.18, and 4.21 compare wide-area and localized excitation at 800Hz and 1200Hz excitation frequency. Mechanical resolution is quantified as Full Width Half Maximum (FWHM) of the gradient of the normalized vibration amplitude (i.e. impulse response) over the FOV. Figure 4.19 and 4.20 show the impulse response at the excitation frequency of 800Hz for wide-area and localized excitation respectively, whereas Figure 4.22 and 4.23 show the impulse response at the excitation frequency of 1200Hz for wide-area and localized excitation respectively. Figure 4.19, 4.20, 4.22 and 4.23 were generated by smoothing (refers to 'smooth' function in MATLAB; degree 0.06 for wide-area and 0.1 for localized which corresponds to averaging of 20μm and 34μm respectively) the gradient of

normalized vibration amplitude (at a single depth over the transverse position) and a first order Gaussian is fitted to the each smoothed impulse response.

Table 4.4: Experimental parameters and phantoms for the comparison of localized vs. wide-area excitation experiments

| Sample | Side-side Silicone and 4% Gelatin sample |
|---|---|
| Number of Ascans | 2048 |
| Field of view (Transverse) | 0.7mm |
| Field of view (Axial) | 2mm |
| Excitation Frequency | 600Hz - 1200Hz |

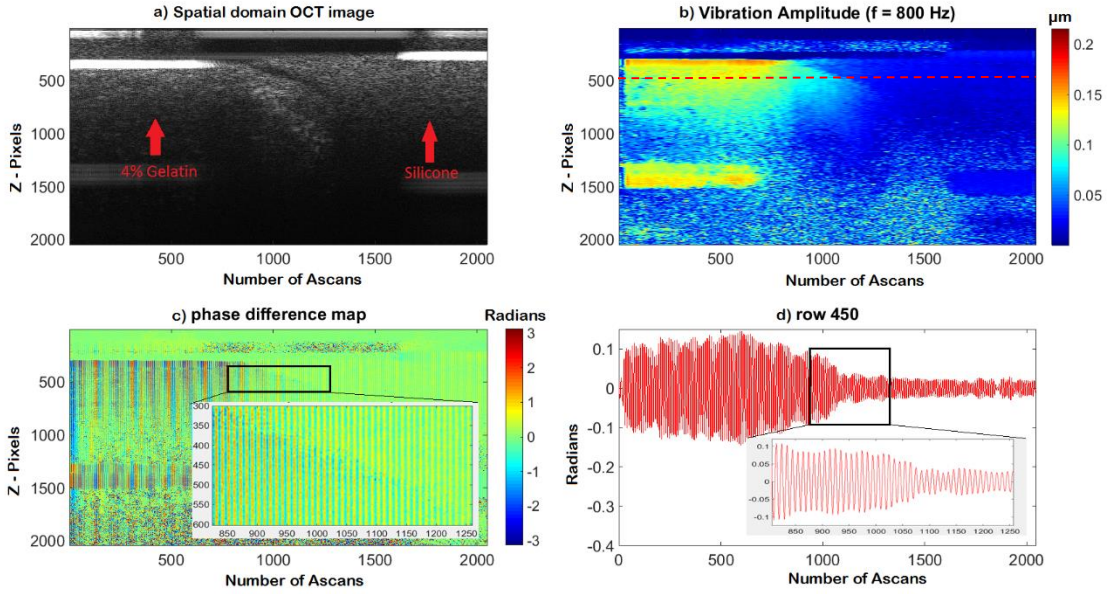


Figure 4.14 : Wide-area excitation at 800Hz excitation frequency on a side-side 4% gelatin - silicone sample (The dashed red line refers to the row plotted in Figure 4.18).

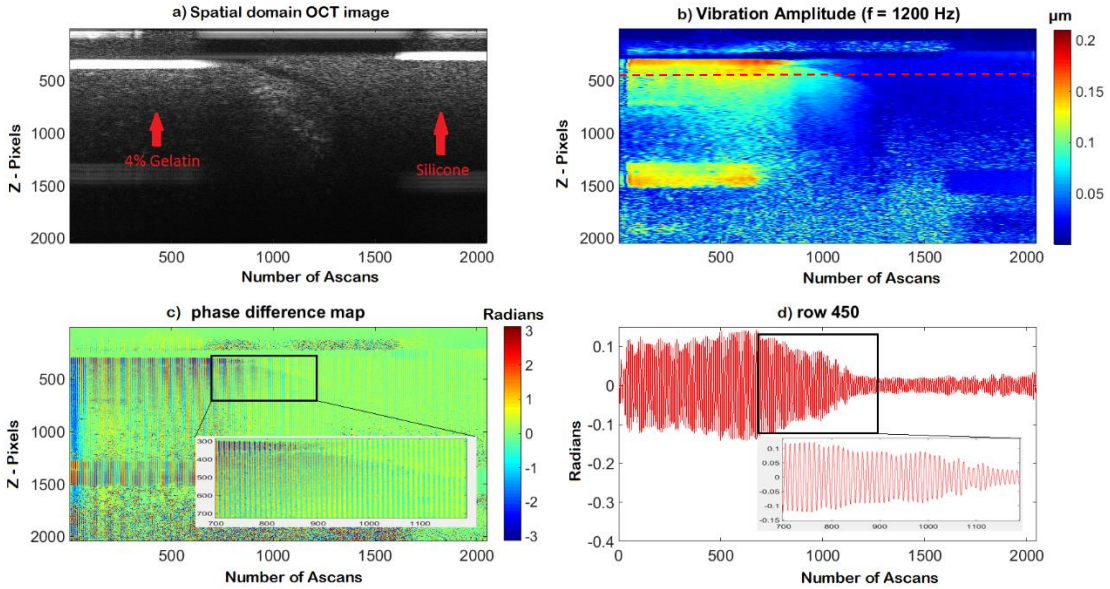


Figure 4.15 : Wide-area excitation at 1200Hz excitation frequency on a side-side 4% gelatin - silicone sample (The dashed red line refers to the row plotted in Figure 4.20).

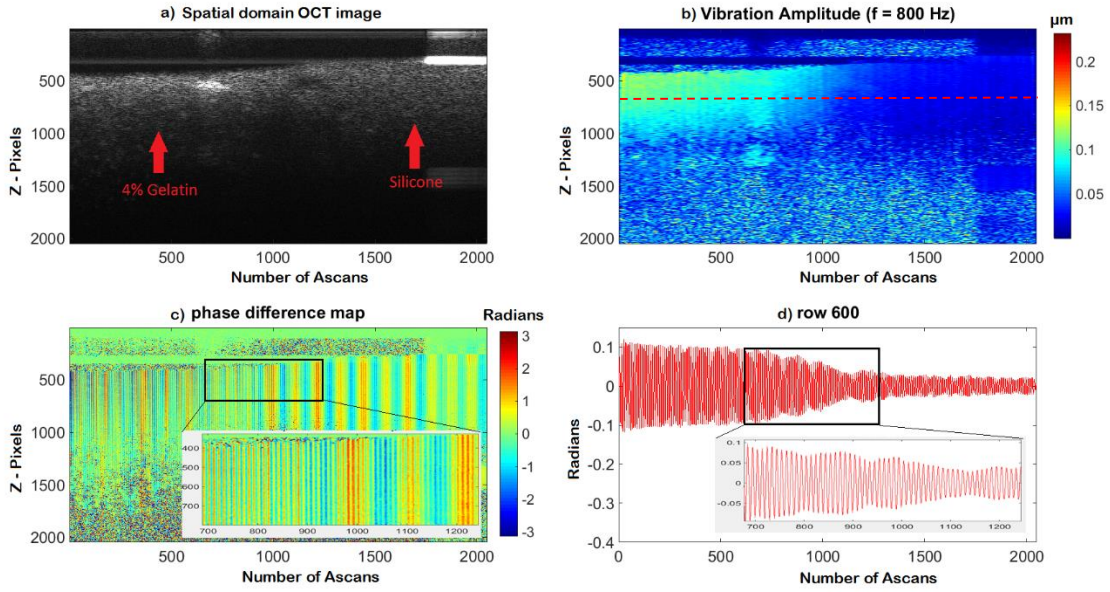


Figure 4.16 : Localized excitation with stage scanning at 800Hz excitation frequency on a side-side 4% gelatin - silicone sample (The dashed red line refers to the row plotted in Figure 4.18)

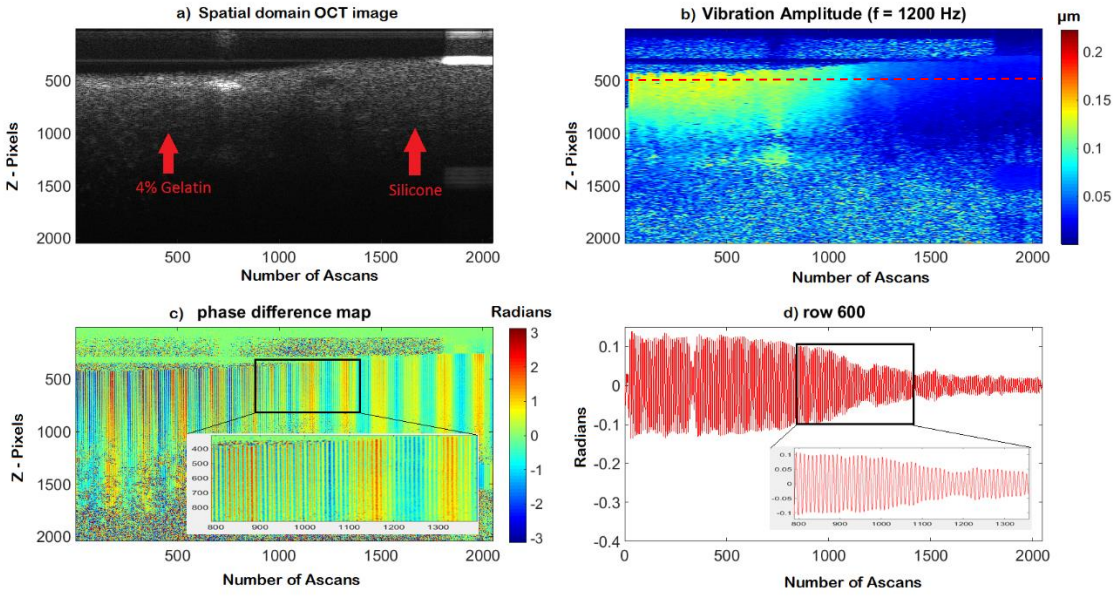


Figure 4.17 : Localized excitation with stage scanning at 1200Hz excitation frequency on a side-side 4% gelatin - silicone sample (The dashed red line refers to the row plotted in Figure 4.20)

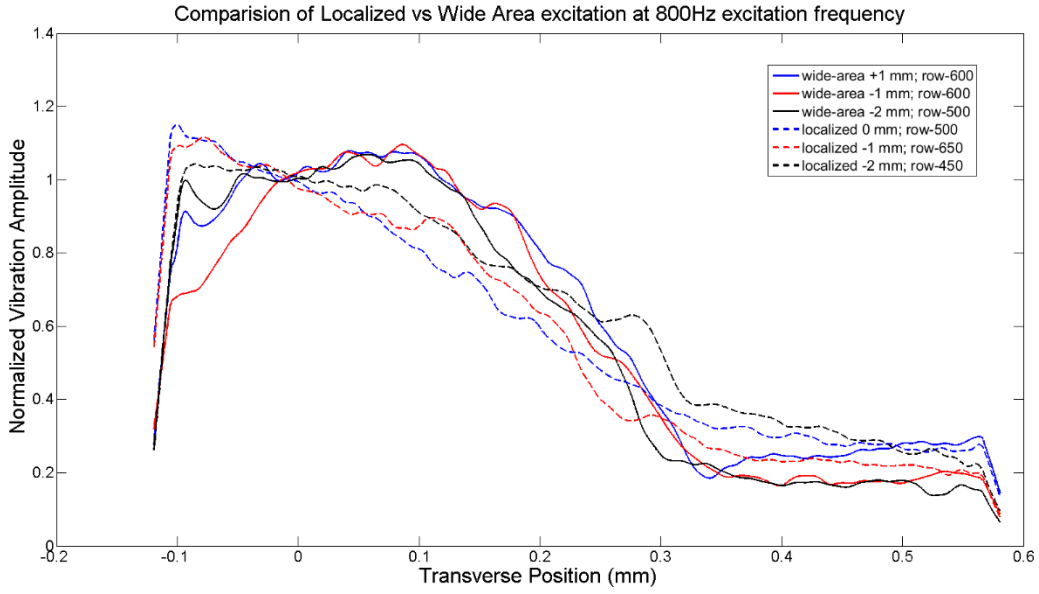


Figure 4.18 : Comparison of localized excitation with stage scanning versus wide-area excitation at 800Hz excitation frequency at 3 different locations on a side-side 4% gelatin - silicone sample

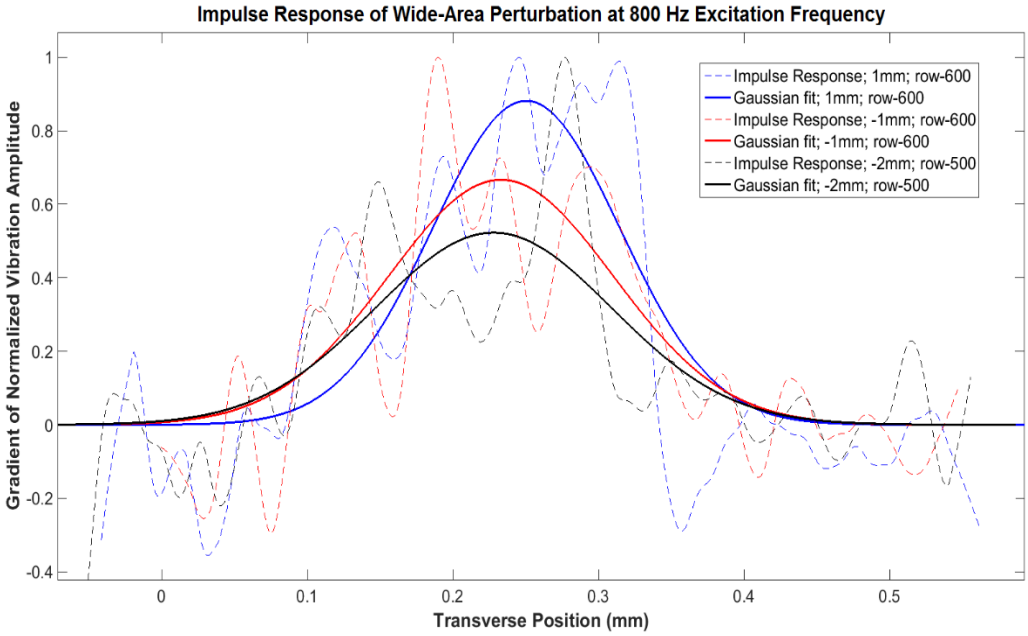


Figure 4.19 : Impulse response of wide-area excitation and corresponding first order Gaussian fit at 800Hz excitation frequency at 3 different locations on a side-side 4% gelatin - silicone sample

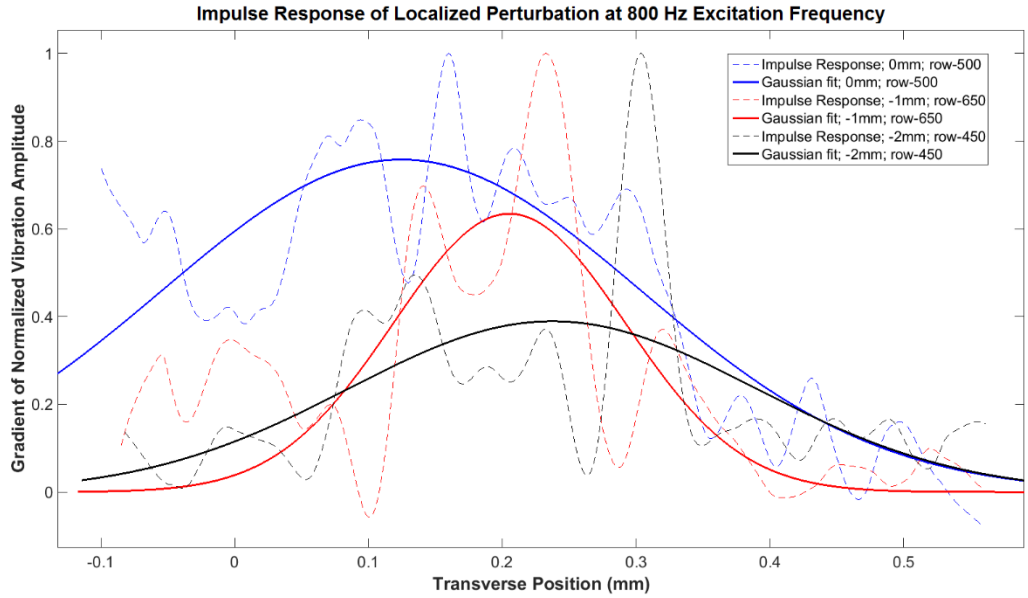


Figure 4.20 : Impulse response of localized excitation and corresponding first order Gaussian fit at 800Hz excitation frequency at 3 different locations on a side-side 4% gelatin - silicone sample

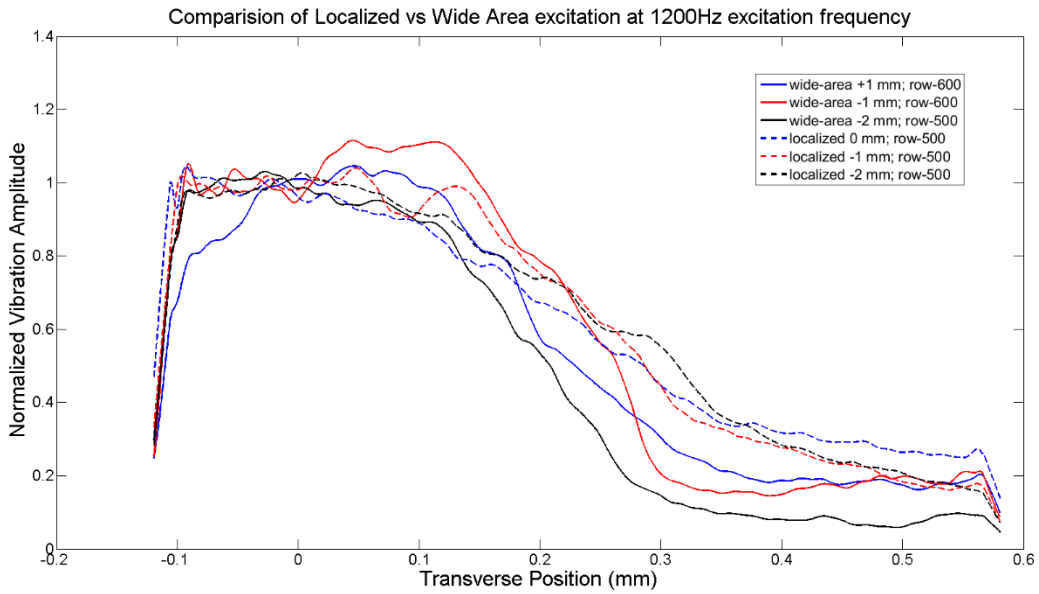


Figure 4.21 : Comparison of localized excitation with stage scanning versus wide-area excitation at 1200Hz excitation frequency at 3 different locations on a side-side 4% gelatin - silicone sample

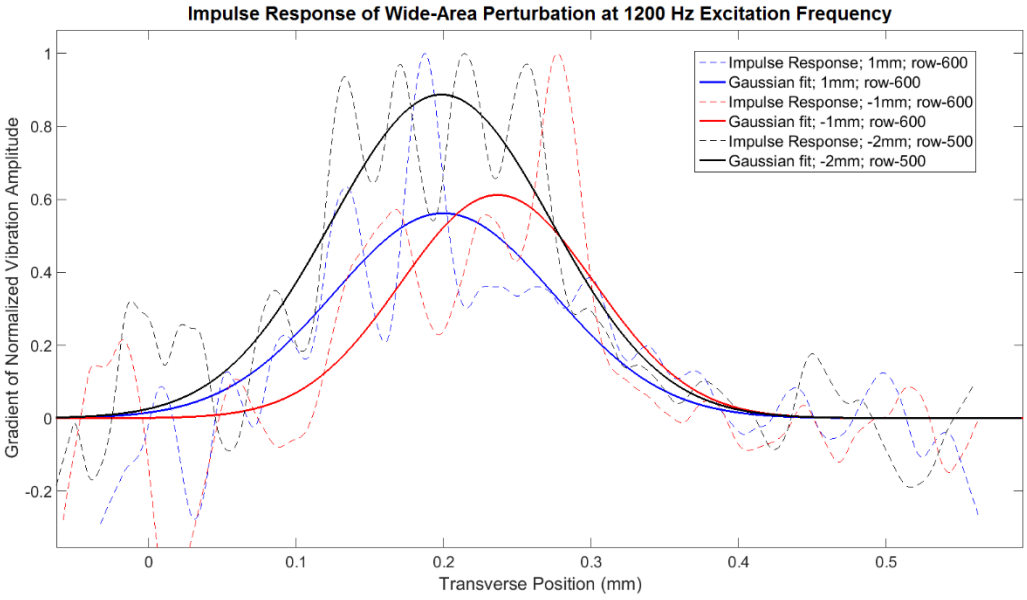


Figure 4.22 : Impulse response of wide-area excitation and corresponding first order Gaussian fit at 1200Hz excitation frequency at 3 different locations on a side-side 4% gelatin - silicone sample

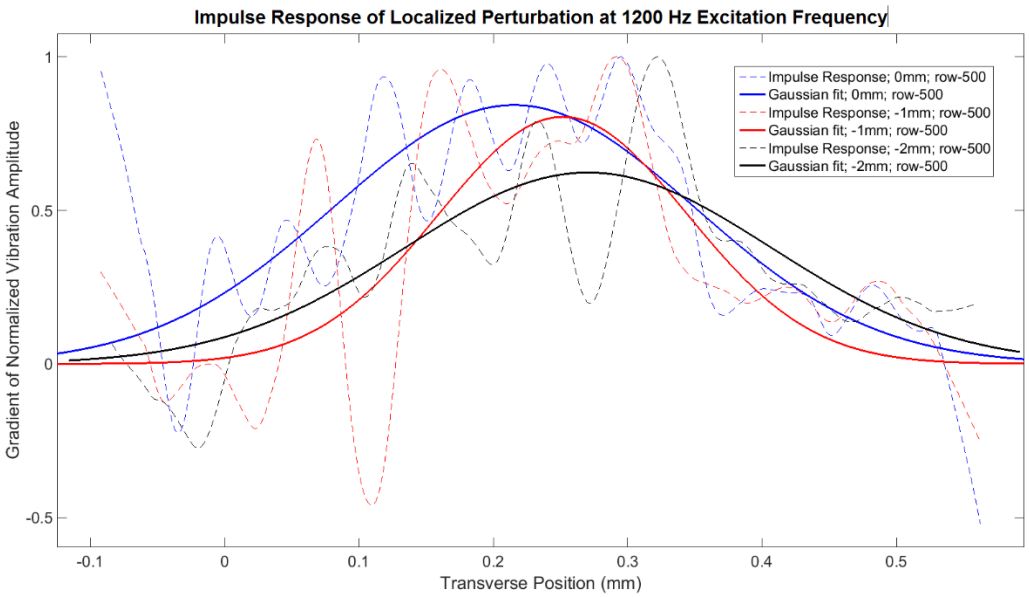


Figure 4.23 : Impulse response of localized excitation and corresponding first order Gaussian fit at 1200Hz excitation frequency at 3 different locations on a side-side 4% gelatin - silicone sample

Table 4.5: Mechanical resolution for localized excitation with stage scanning and wide-area excitation at three different locations on a side-side 4% gelatin - silicone sample at excitation frequencies of 800Hz and 1200Hz respectively (M.R. refers to Mechanical resolution)

| Excitation Frequency | 800Hz | | | 1200Hz | | |
|---|---|---|---|---|---|---|
| Experiment number | 1 | 2 | 3 | 1 | 2 | 3 |
| M.R of wide-area excitation (µm) | 152 | 182 | 192 | 176 | 155 | 176 |
| Average Mechanical Resolution (µm) | 175.3 | | | 169 | | |
| M.R. of localized excitation (µm) | 420 | 204 | 475 | 316 | 218 | 321 |
| Average Mechanical Resolution (µm) | 366.3 | | | 285 | | |

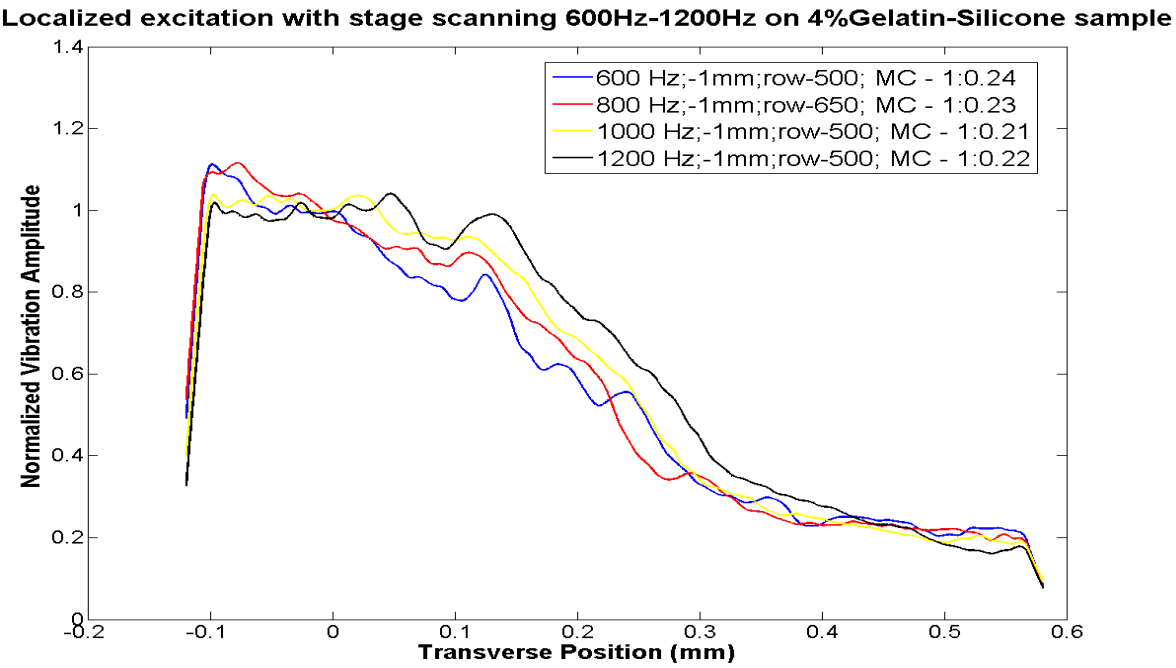


Figure 4.24 : Frequency dependent localized excitation at excitation frequencies 600Hz to 1200Hz on a side-side 4% gelatin - silicone sample (MC refers to Mechanical Contrast)

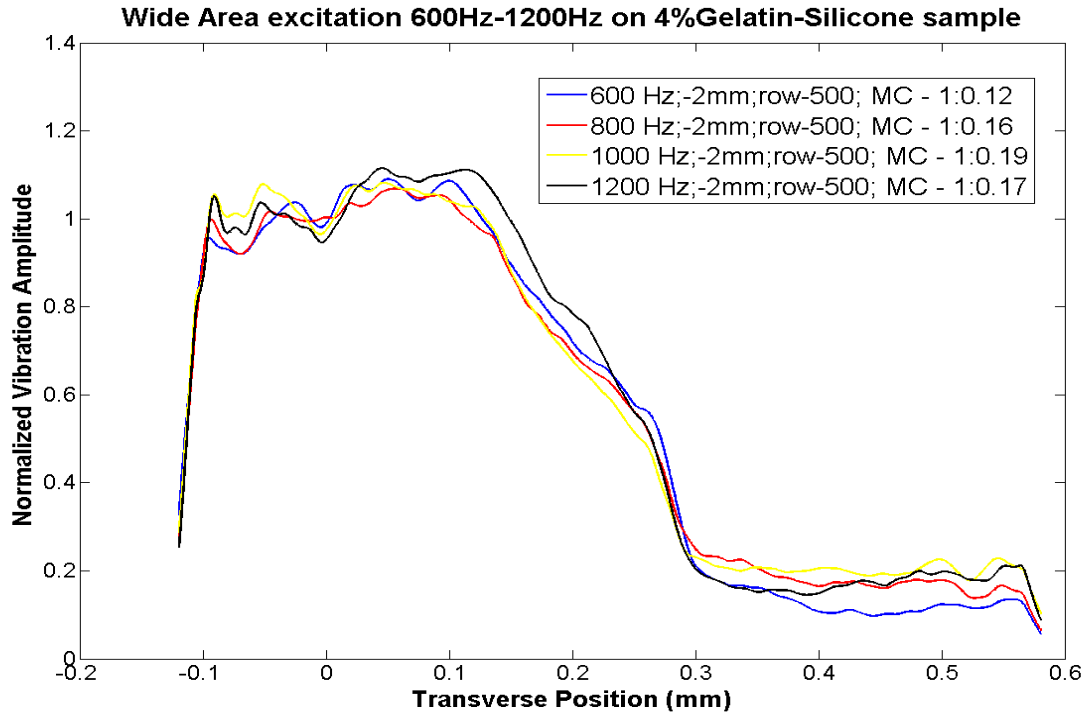


Figure 4.25 : Frequency dependent wide-area excitation at excitation frequencies 600Hz to 1200Hz on a side-side 4% gelatin - silicone sample (MC refers to Mechanical Contrast)

### *4.5 Discussion and future work*

From the experimental results, wide-area excitation provides a better mechanical resolution than localized excitation (see Table 4.5) which is in contrary to the hypothesis in the literature [5]. All the experimental parameters were kept the same (see Equation 3.3) and optimal filtering was done to eliminate stray frequency components. The side-side gelatin sample does not provide a sharp mechanical boundary between the regions of different stiffness due to mixing. So silicone - gelatin sample has been used but even with such a sample, the potential advantages of localized excitation were not seen. One drawback of silicone gelatin sample is that silicone is hydrophobic and it doesn't couple well with gelatin. One suggestion is to make a side-side silicone sample with different stiffness which is not easier to make (mechanically coupled one's) since silicone sample needs to be baked at high temperature to solidify but gelatin once cooked, solidifies at room temperature. The frequency dependence of mechanical contrast was clearly seen for both localized and wide-area excitation in a side-side gelatin sample (see Figure 4.6 and 4.11) but not in a silicone gelatin sample (see Figure 4.24 and 4.25). One of the possible reason could be that silicone and gelatin are not mechanically coupled. It is important to have a sample that is mechanically coupled but with a sharp boundary between heterogeneities for establishing this validation.

Even though the potential advantages of localized excitation over wider area excitation in terms of mechanical resolution is not seen, there are other individual advantages of using both these excitation methods. With localized excitation, higher excitation frequency can be used and thereby a higher mechanical contrast. Due to higher attenuation at higher excitation frequencies, the perturbation would be more localized and it is expected to reduce the artifacts from reflections. In localized excitation with stage scanning, the field of view depends on the distance covered by the motorized stage (with a limitation to maintain the average power of the ultrasound transducer) but

in wide-area excitation it depends on the spot size of the transducer. This is shown in Figure 4.26 where localized excitation with stage scanning at 1200Hz on a side-side 20%-4% gelatin sample is done with FOV of 2 mm (both transverse and axial). Despite other drawbacks, the wide-area perturbation method has a simple setup and can be translated to clinical settings easily. The localized excitation setup needs the motorized translation stage to be synchronized with imaging system. The motion of the stage gives rise to stray frequency components. One other drawback of localized excitation is that due to stray frequencies from scanning of motorized stage, obtaining the mechanical response from the excitation frequencies of 400 Hz or less is not possible even with optimal filtering. As seen in Figure 4.24 it is possible to obtain dataset only from 600Hz. But for wide-area, even lower frequency excitation mechanical response (from 200 Hz) can be obtained. It is not shown in Figure 4.25 in order to provide a direct comparison with localized excitation but can be seen in Figure 4.11.

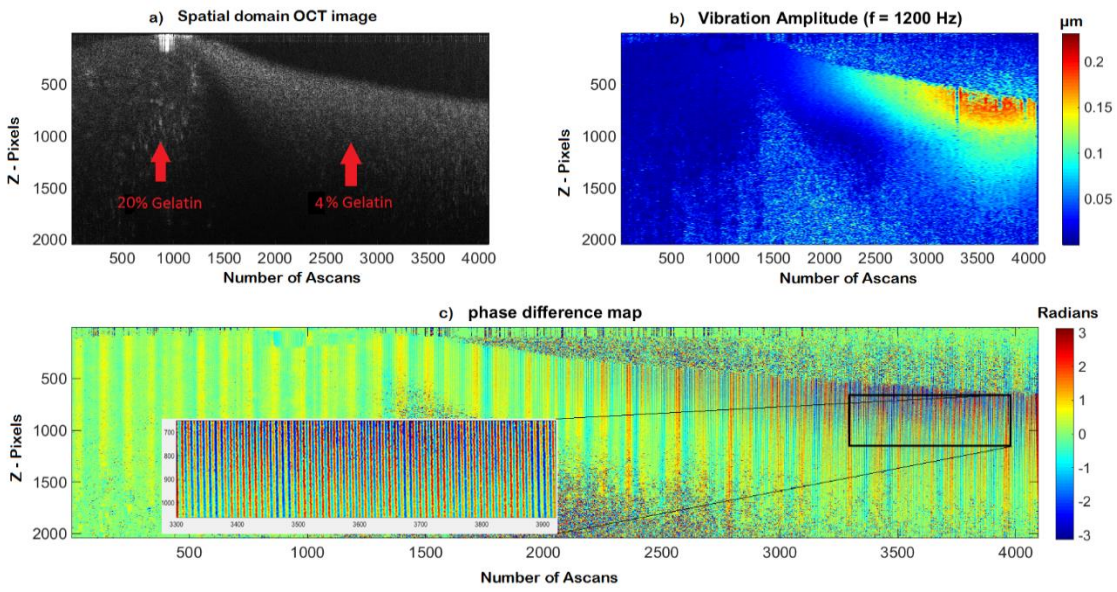


Figure 4.26 : Localized excitation with stage scanning at 1200Hz excitation frequency on a side-side 20%-4% gelatin sample with a FOV of 2.156mm.

Based on the experimental results on the 4% gelatin- silicone side by side sample, the wide-area excitation has better mechanical resolution and mechanical contrast when compared to localized excitation/ remote palpation. Next step is to provide a hypothesis that explains the phenomenon (i.e. better mechanical resolution and contrast from wide-are excitation) seen in the experimental results.

The results shown in this thesis are qualitative but there is a strong need to quantify the mechanical response (i.e. displacement) in terms of complex shear modulus. The ratio of stiffness in terms of shear modulus from indentation for side-side 4% gelatin and silicone sample is 1:25 [24][25] but the average mechanical contrast (in terms of displacement) from experiments for wide-area and localized excitation are in the ratio of 1:0.1585 and 1:0.226 respectively (see Figure 4.24 and 4.25). One advantage of localized excitation over the wide-area excitation with regards to quantifying the biomechanical properties is that with localized excitation, the model independent reconstruction of complex shear modulus can be done [18]. Localized excitation with stage scanning allows us to calculate phase delay between the driving waveform and strain response. The reconstruction method is discussed in depth in section 2.8.1. Finite element modelling is also needed to complement these results and to provide additional information. Finally it is important to work on real samples to improve the existing diagnostic capability and translate the technology to clinical settings.

# 5. CONCLUSION

- The mechanical interaction length reduces with increase in excitation frequency and the mechanical contrast improves with increase in excitation frequency.

- There is no clear demonstration that localized excitation is better than wide-area excitation in terms of mechanical resolution and contrast even with a phantom providing sharp mechanical boundary. Experimental results demonstrate wide-area excitation has better mechanical resolution and contrast. Further investigation is needed using better phantoms and using FEM to study the effects.

- Localized excitation with stage scanning has some other advantages such as large FOV due to stage scanning, can use higher excitation frequency thereby better mechanical contrast and reduce artefacts from the boundary.

- Wide-area excitation has a simple setup and it can be easily translated to clinical settings with a confocal setup.

- The ARF intensity from wide-area excitation is within the FDA limit (0.72 $W/cm^2$) and the intensity from localized excitation exceeds the limit by 3 times approximately.

- Localized excitation allows model independent reconstruction of complex shear modulus.

# APPENDIX A

***Procedure to do ARF-OCE experiments***

1. Follow the steps from the "steps to take an OCT image" document to setup the sample and take an OCT image.

2. For the focused transducer put the focus of the ultrasound beam to the top surface of the sample. Using pulser receiver maximize the sent ping pulse's reflection from the top surface of the sample. For a wide-area transducer, keep the transducer as close as possible to the sample.

3. Set the function generator to modulation, external, frequency - 10 MHz (varies according to the transducer), In the LabVIEW, turn the modulation on and set it to A, set the modulation amplitude as 1.7, wait time between frames as 1 second (to maintain the average power of 125mW), modulation depth in function generator such that ARF reaches zero (approx. 104.5%). Attenuate the signal from the function generator (23 dB attenuator) and then send it to the power amplifier (55 dB power amplifier). From the power amplifier connect it to the ultrasound transducer. One important thing is to run the LabVIEW program once without turning on the power amplifier with the above mentioned settings. During the experiment it is important to look the power amplifier every time to check whether the average power is maintained since sometimes the settings gets changed when the imaging ends.

4. Now align the optical beam and the acoustic radiation force from the transducer to the same transverse location. The coarse alignment is done such that to maximize the amplitude of the phase difference in k-space from background subtraction in LabVIEW. The fine adjustment is done in MATLAB post processing to align the area of impact to the centre of imaging window.

5. For localized excitation with stage scanning move the ultrasound transducer such that the area of impact is at the end of imaging frame (half the FOV to the left of the imaging window depending on the galvo scanning direction x or y). Set the wait time between frames as 0.33. Increase the buffer when increasing the number of A-scans and similarly reduce the buffer when using A-scan rate of 4 kHz and less. The stage scanning introduces stray frequency components which can be compensated by bandwidth filter in post processing. Use the scan center x and y in LabVIEW to move to the different locations of the sample.

6. After taking a dataset, process it immediately to check whether the vibration amplitude is enough and avoid any phase wrapping issues.

# APPENDIX B

***Supplemental material in cd***

Includes

- Datasheets, tech sheets and quotations for power amplifier ENI 3100LA, motorized stage (Newport XPS Q-2), Olympus IMS - ultrasound transducer and materials for making phantoms.
- Post processing MATLAB code
- LabVIEW application
- Results

# BIBILIOGRAPHY


[1] K. J. Parker, "Imaging Elastic Properties of Tissue," in *Emerging Imaging Technologies in Medicine*, M. A. Anastasio and P. La Riviere, Eds. CRC Press, Taylor and Francis group, 2013, pp. 183–200.

[2] M. M. Doyley, "Model-based elastography: a survey of approaches to the inverse elasticity problem," *Phys. Med. Biol.*, vol. 57, no. 3, pp. R35–R73, Feb. 2012.

[3] J. a. Mulligan, G. R. Untracht, S. N. Chandrasekaran, C. N. Brown, and S. G. Adie, "Emerging Approaches for High-Resolution Imaging of Tissue Biomechanics With Optical Coherence Elastography," *IEEE J. Sel. Top. Quantum Electron.*, vol. 22, no. 3, pp. 1–20, 2016.

[4] Y. Wang, S. Adie, S. Boppart, and M. Insana, "Ultrasound and Optical Methods for Dynamic Viscoelastic Imaging," in *Handbook of Imaging in Biological Mechanics*, CRC Press, 2014, pp. 83–96.

[5] K. R. Nightingale, M. L. Palmeri, R. W. Nightingale, and G. E. Trahey, "On the feasibility of remote palpation using acoustic radiation force.," *J. Acoust. Soc. Am.*, vol. 110, no. 1, pp. 625–634, 2001.

[6] J. J. Dahl, "Acoustic Radiation Force Imaging," in *Emerging Imaging Technologies in Medicine*, M. Anastasio and P. La Riviere, Eds. CRC Press, Taylor and Francis group, 2013, pp. 201–217.

[7] K. J. Parker, M. M. Doyley, and D. J. Rubens, "Corrigendum: Imaging the elastic properties of tissue: the 20 year perspective," *Phys. Med. Biol.*, vol. 57, no. 16, pp. 5359–5360, Aug. 2012.

[8] M. Razani, A. Mariampillai, C. Sun, V. X. D. Yang, and M. C. Kolios, "Biomechanical properties of soft tissue measurement using optical coherence elastography," vol. 8207, no. 1, pp. 820758–820758–8, Feb. 2012.

[9] B. F. Kennedy, T. R. Hillman, R. A. Mclaughlin, B. C. Quirk, and D. D. Sampson, "In vivo dynamic optical coherence elastography using a ring actuator," vol. 17, no. 24, pp. 556–562, 2009.

[10] B. F. Kennedy, K. M. Kennedy, and D. D. Sampson, "A Review of Optical Coherence Elastography: Fundamentals, Techniques and Prospects," *IEEE J. Sel. Top. Quantum Electron.*, vol. 20, no. 2, pp. 272–288, Mar. 2014.

[11] Y. K. Mariappan, K. J. Glaser, and Richard L Ehman, "Magnetic Resonance Elastography: a Review," vol. 23, no. 5, pp. 497–511, 2010.

[12] M. J. Paszek, N. Zahir, K. R. Johnson, J. N. Lakins, G. I. Rozenberg, A. Gefen, C. a. Reinhart-King, S. S. Margulies, M. Dembo, D. Boettiger, D. a. Hammer, and V. M. Weaver, "Tensional homeostasis and the malignant phenotype," *Cancer Cell*, vol. 8, no. 3, pp. 241–254, 2005.

[13] J. M. Schmitt, "Optical coherence tomography (OCT): a review," *IEEE J. Sel. Top. Quantum Electron.*, vol. 5, no. 4, pp. 1205–1215, 1999.

[14] W. Drexler and J. G. Fujimoto, *Optical Coherence Tomography: Technology and Applications*. Springer, 2008.

[15] S. G. Adie, B. W. Graf, a. Ahmad, P. S. Carney, and S. a. Boppart, "Computational adaptive optics for broadband optical interferometric tomography of biological tissue," *Proc. Natl. Acad. Sci.*, vol. 109, no. 19, pp. 7175–7180, 2012.

[16] T. Nguyen, E. Y. Wong, R. K. Wang, M. O. Donnell, S. Song, B. Arnal, and Z. Huang, "Shear wave pulse compression for dynamic elastography using phase- sensitive optical coherence tomography elastography using phase-sensitive optical."

[17] V. Crecea, A. Ahmad, and S. a Boppart, "Magnetomotive optical coherence elastography for microrheology of biological tissues.," *J. Biomed. Opt.*, vol. 18, no. 12, p. 121504, 2013.

[18] J. Vappou, C. Maleke, and E. E. Konofagou, "Quantitative viscoelastic parameters measured by harmonic motion imaging.," *Phys. Med. Biol.*, vol. 54, no. 11, pp. 3579–3594, Jun. 2009.

[19] E. L. Carstensen and K. J. Parker, "Physical models of tissue in shear fields.," *Ultrasound Med. Biol.*, vol. 40, no. 4, pp. 655–74, Apr. 2014.

[20] N. Ozkaya, "Fundamentals of Biomechanics," in *Fundamentals of Biomechanics: Equilibrium, Motion and Deformation*, Springer, 2012, pp. 221–228.

[21] Y. Zheng, X. Chen, A. Yao, H. Lin, Y. Shen, and Y. Zhu, "Shear Wave Propagation in Soft Tissue and Ultrasound Vibrometry," *Tech*, pp. 1–24, 2013.

[22] Y. Wang, N. D. Shemonski, S. G. Adie, S. a. Boppart, and M. F. Insana, "Dynamic method of optical coherence elastography in determining viscoelasticity of polymers and tissues," *Proc. Annu. Int. Conf. IEEE Eng. Med. Biol. Soc. EMBS*, pp. 117–120, 2013.

[23] R. K. Manapuram, S. Aglyamov, F. M. Menodiado, M. Mashiatulla, S. Wang, S. a. Baranov, J. Li, S. Emelianov, and K. V. Larin, "Estimation of shear wave velocity in gelatin phantoms utilizing PhS-SSOCT," *Laser Phys.*, vol. 22, no. 9, pp. 1439–1444, 2012.

[24] M. Orescanin, K. S. Toohey, and M. F. Insana, “Quantitative shear wave imaging of cell culture gels,” *Proc. - IEEE Ultrason. Symp.*, pp. 2–5, 2009.

[25] X. Liang, A. L. Oldenburg, V. Crecea, E. J. Chaney, and S. a Boppart, “Optical micro-scale mapping of dynamic biomechanical tissue properties.,” *Opt. Express*, vol. 16, no. 15, pp. 11052–11065, 2008.

[26] M. Orescanin, K. S. Toohey, and M. F. Insana, “Material properties from acoustic radiation force step response.,” *J. Acoust. Soc. Am.*, vol. 125, no. 5, pp. 2928–2936, 2009.

[27] S. G. Adie, X. Liang, B. F. Kennedy, R. John, D. D. Sampson, and S. A. Boppart, “Spectroscopic optical coherence elastography,” vol. 18, no. 25, pp. 63–73, 2010.